Computation of the MARS test simulating a Hypothetical Core Disruptive Accident in a small scale replica of a Fast Breeder Reactor

Marie-France Robbe, Jean-Yves Cariou, Michel Lepareux, Eloi Treille

Computation of the MARS test simulating a Hypothetical Core Disruptive Accident in a small scale replica of a Fast Breeder Reactor

M.F. Robbe
CEA Saclay, DRN-DMT-SEMT, 91191 Gif sur Yvette cedex, France
Tel: (33) 1 69 08 87 49, Fax: (33) 1 69 08 52 42, E-mail: mfrobbe@cea.fr
Y. Cariou
Novatome, NVPM, 10 rue Juliette Récamier, 69006 Lyon, France
M. Lepareux
CEA Saclay, DRN-DMT-SEMT, 91191 Gif sur Yvette cedex, France
E. Treille
Socotec Industrie, 1 av. du Parc, 78180 Montigny le Bretonneux, France

Abstract

In case of a Hypothetical Core Disruptive Accident (HCDA) in a Liquid Metal Reactor, the interaction between fuel and liquid sodium creates a high pressure gas bubble in the core. The violent expansion of this bubble loads the vessel and the internal structures, whose deformation is important. The experimental test MARS simulates a HCDA in a small scale mock-up containing all the significant internal components of a Fast Breeder Reactor. The test-facility is filled with water topped by an argon blanket and the explosion is generated by an explosive charge.

This paper presents a numerical simulation of the test with the CASTEM-PLEXUS code. The top closure is represented by massive structures. The main internal structures are described by shells while the peripheral massive structures are taken into account with a pressure loss because their geometry is too complicated to mesh them.

1 INTRODUCTION

In case of a Hypothetical Core Disruptive Accident (HCDA) in a Liquid Metal Reactor, the interaction between fuel and liquid sodium creates a high pressure gas bubble in the core. The violent expansion of this bubble loads the vessel and the internal structures, whose deformation is important.

During the 70s and 80s, the LMFBR integrity was studied with codes specially devoted to the analysis of transient loads resulting from a HCDA : PISCES 2 DELK (Cowler, 1979), REXCO (Chang, 1974), MICE, ICECO, ICEPEL, STRAW and SADCAT (Chang, 1977), SURBOUM (Stiévenart, 1975), SEURBNUK/EURDYN (Cameron, 1977) (Smith, 1983) (Smith, 1987), ASTARTE (Cigarini, 1983), CASSIOPEE (Graveleau, 1979), SIRIUS...

In order to validate these codes, experimental programmes and benchmarks were undertaken by several countries : COVA (Hoskin, 1978) (Holtbecker, 1977) (Albertini, 1984) (Wenger, 1987) (Kendall, 1980), APRICOT (West, 1980), WINCON (Sidoli, 1988), STROVA (Kendall, 1986), CONT (Benuzzi, 1987), MARA...

The french code SIRIUS (Blanchet, 1981) (Daneri, 1981) (Acker, 1981) was validated on the french experimental programme MARA (Louvet, 1989) (Bour, 1989). Based on a 1/30 scale model of the Superphenix reactor, the French programme MARA-MARS involved eleven tests of gradual complexity due to the addition of internal deformable structures:

- MARA 1 and 2 considered a vessel partially filled with water and closed by a rigid roof (Acker, 1981),
- MARA 4 represented the main core support structures (Smith, 1985),
- MARA 8 and 9 were closed by a flexible roof (Fiche, 1985),
- MARA 10 included the core support structures (CSS) and a simplified representation of the above core structure (ACS) (Louvet, 1987).

The MARS test (Falgayrettes, 1983) rested on a 1/20 scale mock-up (Fig. 1) including all the significant internal components.

As other codes using a Lagrangian approach, SIRIUS needed rezonings during calculation because the internal structure presence caused high distortion of the fluid meshes. Finite differences were used for the sodium and the roof and finite elements for the thin vessel. As the argon and the bubble were not meshed, a law related volume to pressure.

At the end of the 80s, it was preferred to add a specific HCDA sodium-bubble-argon tri-component constitutive law (Lepareux, 1991) to the general ALE fast dynamics finite element CASTEM-PLEXUS code. The HCDA constitutive law was qualified (Casadei, 1989) on the CONT benchmark.

In order to demonstrate the CASTEM-PLEXUS capability to predict the behaviour of real reactors (Lepareux, 1993) (Cariou[a], 1997), axisymmetric computations of the MARA series were confronted with the experimental results. The computations performed at the beginning of the 90s showed a rather good agreement between the experimental and computed results for the MARA 8 and MARA 10 tests even if there were some discrepancies (Cariou, 1993). On the contrary, the prediction of the MARS structure displacements and strains was overestimated (Cariou[b], 1997).

As the process used for dealing with the fluid-structure coupling was improved since then and as this process improved the precision of the results for the tests MARA8 and MARA10, it was undertaken another comparison between the experimental results of the MARS test with a finer size of the mesh.

This paper presents the numerical simulation of the MARS test with the CASTEM-PLEXUS code. The top closure is represented by massive structures. The main internal structures are described by shells while the peripheral massive structures are taken into account with a pressure loss because their geometry is too complicated to mesh them. The computation uses the new process for the fluid-structure treatment. The paper is focused on the numerical models, the analysis of the results computed by the code CASTEM-PLEXUS.

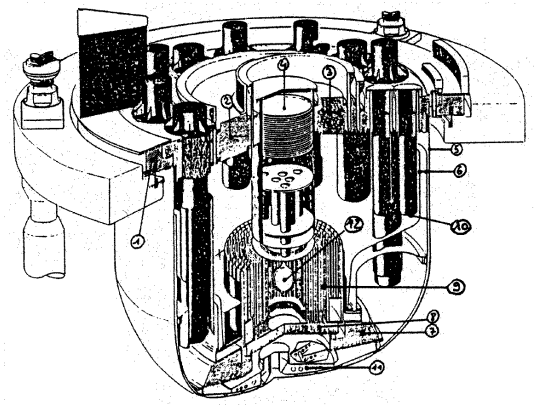

mark 1: roof
mark 2: large rotating plug
mark 3: small rotating plug
mark 4: core cover plug
mark 5: main vessel
mark 6: internal vessels
mark 7: core support structures
mark 8: diagrid support
mark 9: core and neutron shieldings
mark 10: pumps and heat exchangers
mark 11: core catcher

Fig. 1: The MARS test-facility

2 ANALYSIS OF THE RESULTS

The results are described through the evolution of several variables versus time: pressure, gas presence fraction, fluid speed, deformed shape of the mesh and of the structures, radial and vertical displacements of the structures, stresses and strains in the structures.

2.1 Pressure

The figure 2 presents the pressure versus time in the whole mock-up. Initially, the water and argon are at the atmospheric pressure whereas the explosive charge simulating the bubble gas is at 288 MPa. From 0.02 ms, a pressure wave issued from the bubble zone expands spherically.

At 0.06 ms, the pressure wave hits the nearest structures: the lateral shielding, the in-pile shell of the Core Cover Plug (CCP) and the diagrid. At 0.1 ms, the pressure wave has gone farther than the central structures and impacts the baffle and the second spacer plate of the CCP. In a first time, the diagrid holds back the propagation of the pressure wave. The pressure level has fallen to approximately 60 MPa at 0.1 ms.

After 0.14 ms, the pressure wave succeeds in accelerating the water below the diagrid and the pressure wave continues its progression downwards but with a lower level of 12 MPa. In the upper part, the pressure wave continues its spherical propagation and impacts the lower part of the internal vessel. At 0.18 ms, the pressure wave hits the upper spacer plate of the CCP. The highest pressure is located in the bottom of the central zone because of the confinement imposed by the nearest structures. Consequently the lateral shielding and the diagrid are the structures most in demand. A small depressurisation appears in the centre of the initial bubble zone and between the in-pile shell and the lower spacer plate of the CCP.

The pressure wave keeps a spherical shape until 0.22 ms. From 0.26 ms, the shape of the pressurised wave changes because of its progression is limited by the main vessel at the bottom and the presence of the argon layer at the top. Depressurised zones are created in the bottom of the central zone (previously the most pressurised water area) and in the middle of the CCP. At 0.26 ms, the pressure wave impacts the bottom of the main vessel.

At 0.3 ms, the pressure wave has completely gone round the Core Support Structure and hits the upper part of the torospherical part of the main vessel. The maximum pressure is 25 MPa below the diagrid and 18 MPa at the level of the internal vessel. The bottom of the central zone, the bottom of the space between the lateral shielding and the baffle and the CCP top are depressurised. The argon layer always remains at a low pressure because of the compressibility of the gas.

At 0.34 ms, the pressure wave continues its lateral progression and hits the cylindrical side of the main vessel. Since 0.38 ms, the average pressure is much lower in the whole mock-up. The maximum pressure is 12 MPa in the central zone and against the top of the internal vessel. Indeed the lateral development of the pressure wave leads to a sort of queue which impacts the intermediate and the upper part of the internal vessel.

From 0.42 to 0.8 ms, the highest pressure remains located in the central confined zone but the maximum level is no more than 10 MPa. Globally, the pressurised areas are concentrated in the central zone, between the radial shielding and the internal vessel lower part and later in the Core Cover Plug and against the main vessel.

Between 1.2 and 3.2 ms, the pressure decreases in the central zone, below the diagrid and in the CCP. The pressurised area next to the main vessel goes up progressively along the vessel and then it is pushed back towards the inner part of the test-facility. At 3.4 ms, the pressurised fluid concentrates in the top of the CCP because the perforated external cylinder surrounding the CCP favours the passing of fluid and thus of the pressure wave from outside to inside the CCP. The initial argon zone near the CCP becomes pressurised because of the invasion of this gaseous zone by the water.

From 3.4 to 4.7 ms, the pressure wave rebounds in the corner formed by the lower the heat-insulation plate topping the CCP. The pressure wave is then pushed back following the top closure (small and large rotating plugs and roof slab) towards the main vessel. The top layer initially filled with argon is become as pressurised as the rest of the mock-up because the argon was pushed out of this zone by the pressurised water.

Between 4.7 and 6.2 ms, the pressure wave successively impacts the upper part of the main vessel, rebounds against the top corner at the junction of the main vessel with the roof slab, then goes down following the main vessel and concentrates between the Core Support Structure and the internal vessel. Afterwards, the pressure is lower than 5 MPa and the following rebounds of the pressure wave are more difficult to detect.

2.2 Gas fraction

The figures 3 to 5 show respectively the general volumic presence fraction of the gas, the massic presence fractions of the bubble and of the argon. Initially, the mock-up is filled with liquid water except in the centre where is located the explosive charge and below the top closure which shelters the argon layer.

Between 0.02 and 0.2 ms, the bubble gas grows spherically and remains in the central area confined by the presence of the diagrid support, lateral neutron shielding and in-pile plate of the core cover plug. At 0.2 ms, the argon layer starts being compressed upwards in the CCP and below the small rotating plug because of the arrival of the pressure wave impacting the top closure.

From 0.4 ms, besides of the expansion of the bubble gas, we observe the vaporisation of water in the areas which become depressurised after the passing of the pressure wave. For instance, the water at the bottom of the central area and at the top of the CCP vaporises at 0.4 ms while the pressure level decreases there until the initial atmospheric pressure.

Between 0.8 and 2 ms, water steams in large areas of the test-facility: below the diagrid, under the top closure, around the internal vessel, above the upper spacer plate in the CCP and also just along the vertical structures (the lateral shielding, the baffle and the lower part of the internal vessel). All these areas are at a low pressure when the water vaporises. But since the pressure increases again, the steam condenses. It is the case in the fluid area below the internal vessel: between 0.8 and 1.2 ms, the water vaporises owing to the very low pressure and since 1.6 ms, the steam condenses because the pressurised area located above the CSS is moving up, thus increasing the local pressure level.

Meanwhile, the pressurised bubble gas continues its expansion in the central area. At 1.2 ms, the bubble gas is shifted upward. The bottom of the central area is filled with liquid water which is trapped by the confinement and the blocking-up due to the bubble growth. In that zone, the steam has condensed due to the pressure increase caused by the bubble expansion. From 1.6 ms, the bubble gas starts escaping out of the central zone by the free channel between the neutron shielding top and the CCP base.

Between 0.2 and 1 ms, the argon layer is progressively compressed upwards against the top closure because of the thrust of the liquid water ejected from the central area and because of the creation of steam just below the argon layer. From 1.6 to 4 ms, the argon is pushed and concentrated in the top corner near the junction of the roof and the main vessel. The arrival of the high pressure bubble gas going out the central area pushes and compresses the low pressure argon gas.

Between 3 and 10 ms, the bubble gas expands out of the central zone. A large panache forms between the external cylinder surrounding the CCP and the internal vessel. Simultaneously, the argon is first compressed in the top corner until 4 ms and then the argon expands along the top closure and along the upper part of the main vessel. This argon expansion is due to the general pressure decrease in the test-facility from 6 ms.

From 3 to 10 ms, the water continues vaporising below the diagrid because of the pressure local fall. On the contrary, the steam condenses in the vicinity of the neutron shielding, the baffle and the internal vessel because the expansion of the bubble gas out of the central zone causes a pressure raise in that area.

From 10 to 17 ms, the bubble gas stops expanding out of the central area due to the formation of a fluid whirlpool between the core cover plug and the internal vessel. Consequently, the bubble gas is pushed back in the central area and expands downwards in this confined zone. At 17 ms, the bubble gas fills almost completely the central area. The trapped water is concentrated at the bottom along the diagrid and the symmetry axis.

The bubble gas which went out of the central zone goes slightly away from the CCP and the neutron shielding top and forms a tore which swirls round in the middle of water. Some gas goes down along the outer side of the neutron shielding and remains trapped between the shielding and the baffle.

Argon continues expanding from the top corner toward the symmetry axis by following the top closure and along the main vessel. Later argon gathers in the CCP top, thus forming a sort of argon bag in the core cover plug and a second bag near the top of the main vessel. This second argon bag is at the origin of the formation of a bulge in the upper part of the main vessel.

Finally, because of the pressure fall below the diagrid and the CSS, water vaporises along the main vessel bottom and under the diagrid.

2.3 Fluid velocity

The figures 6 and 7 show the fluid velocities with vectors to indicate the fluid direction and with a colour map to give an idea of the value of the velocities. The fluid is initially at rest in the whole test-facility. Since 0.02 ms, the bubble gas in the mock-up centre expands spherically with a velocity of 200 m/s.

At 0.1 ms, the bubble gas continues to expand but the speed is no more uniform in all the directions. A very high vertical speed is observed on the symmetry axis because the horizontal blocking condition imposed for the elements of the axis is equivalent to a rigid wall. Therefore the pressure peak along the axis is twice the average pressure in the bubble zone, what explains the high speeds of the bubble elements on the axis.

In the central area limited by the diagrid, the neutron shielding and the in-pile plate of the Core Cover Plug, the velocities decrease in the lower part because of the diagrid presence preventing the downward water flows. On the contrary, the lateral and upward velocities in the central zone remain high. The bubble gas hits the central structures at 0.1 ms.

At 0.16 ms, the pressure wave succeeds in accelerating the water located at the periphery of the central zone (between the neutron shielding and the internal vessel, in the lower part of the core cover plug and running on from the free space between the shielding and the CCP). The water impacts the baffle at about 0.12 ms and the lower part of the internal vessel at 0.16 ms, perpendicularly to the shells. Due to the expansion of the pressurised area, the maximum bubble gas speeds fall to 140 m/s in the free channel.

From 0.2 to 0.3 ms, the bubble gas in the central zone is mainly directed upwards and radially. The bubble gas impacts the neutron shielding with a speed up to 80 m/s. Owing to the diagrid presence the downward motion, the bubble gas begins a rotating movement upward directed. The bubble expansion pushes upwards the in-pile plate of the CCP and radially the shielding which goes away under the fluid thrust. The water moves away spherically in almost the whole mock-up. In the CCP, the water moves upwards and has impacted all the spacer plates at 0.22 ms. The water located under the diagrid starts impacting the vessel bottom at 0.3 ms.

Between 0.38 and 0.46 ms, the water continues its spherical expansion. The water hits the main vessel bottom perpendicularly with an average speed of 30 m/s. Besides, the water impacts the upper part of the main vessel from the collar supporting the CSS to almost the main vessel top. The water impacts progressively all the top closure, starting from the heat-insulation of the CCP with a maximum speed of 40 m/s and hitting next both rotating plugs and the roof slab.

From 0.54 to 0.8 ms, the bubble gas continues expanding in the central area, thus impacting all the central structures. But the bubble gas moves preferentially towards the free channel to escape out of the central area with a speed of about 100 m/s. The water continues moving away spherically and impacting all the structures. In the CCP top, the argon moves away horizontally to leave the CCP.

From 1 to 2.4 ms, the bubble gas goes on escaping by the free channel with velocities up to 90 m/s. The bubble gas continues pushing away the neutron shielding, pushing down the diagrid and pushing up the in-pile shell. Out of the central area, the water hits the baffle and the base of the internal vessel with a perpendicular speed. Below the diagrid, the water moves down towards the vessel bottom and then flows along the main vessel towards the collar.

Below the internal vessel, the water first goes toward the torospherical part of the main vessel and later flows upwards towards the top closure by the channel between the main vessel and the internal vessel. Above the baffle and the internal vessel, the bubble gas expels the water mainly upwards but also laterally towards the upper part of the internal vessel. In the core cover plug, the water remains oriented upwards what makes going the argon out of the CCP. The argon is rejected horizontally towards the top corner.

From 3 to 5 ms, the bubble gas goes out of the central area violently. The highest speeds are observed in the free channel for the bubble gas and in the upper part of the mock-up for the water because the water is accelerated up by the bubble expansion. Below the diagrid, the water flow reverses: the water rebounds on the main vessel and goes back toward the diagrid. Between the neutron shielding and the baffle, some bubble gas and water are pushed down. Below the top closure, the water flows orient progressively towards the top corner. We note high horizontal speeds of about 80 m/s just under the top closure which are due to the argon motion outwards.

From 6 to 8 ms, the bubble gas keeps on being expelled violently (with speed up to 90 m/s) from the central area and extending in the water area above the baffle. Between the neutron shielding and the internal vessel, the trapped bubble gas and water are attracted up by the bubble jet. In the CCP, the water continues to be hurled upwards with slower velocities but we observe a small orientation of water and argon towards the symmetry axis. Along the CCP external cylinder, the bubble gas pushes the fluid towards the symmetry axis.

Under the diagrid, the water moves up towards the diagrid. Below the internal vessel, the water decelerates and changes direction: the water near the internal vessel moves back towards this vessel and the water near the main vessel moves up along the vessel. The concentration, in the channel between both vessels, of water coming from below the internal vessel and of argon coming from the top corner, leads to an outward horizontal thrust of the upper part of the main vessel.

From 9 to 14 ms, a large whirlpool forms above the baffle due to the expulsion of the bubble gas out of the central area. The bubble gas is ejected diagonally through the free channel and then turns down at about mid-radius of the mock-up: the bubble gas progression is stopped by the compression of the liquid water. The whirlpool pulls water from the whole upper part of the mock-up and from the spaces between the neutron shielding and the baffle and between the baffle and the internal vessel. The highest speeds are still noted for the bubble gas jet but they remain limited to 40 m/s.

Simultaneously, a second smaller whirlpool creates in the central zone: the bubble gas moves up towards the free channel but it is partially turned away inwards along the in-pile shell and then downwards along the symmetry axis and then the cycle starts again. Under the diagrid, the water slows down considerably. The water changes direction in the channel limited by both vessels: the water moves down because of the high thrust due to the fluid coming from the roof. Below the internal vessel, the water flows down along the main vessel and is very slowed down elsewhere.

Below the roof, we notice two contradictory fluid flows: along the roof, argon moves outwards whereas, on the element layers below, argon and water are pulled inwards by the large whirlpool. In the CCP, the upwards water flow stops and turns back: the water and argon are then propelled downwards.

Between 15 and 17 ms, the whirlpool turns away independently from the rest of the fluid. The bubble gas in the central area remains confined in that area: the whirlpool prevents the going out of more gas. On the contrary, the whirlpool pushes down fluid inside the confined area. The fluid inside the central area is mainly oriented downwards. Its impact on the diagrid causes a downward motion of the water below the diagrid. As the fluid entering in the central area exerts an upward thrust on the CCP, the water inside the CCP changes direction and moves up once again. At the CCP top, the water escapes out of the CCP whereas the argon concentrates near the symmetry axis.

The whirlpool pulls water and argon from the top closure. The fluid flows down along the internal vessel and along the external cylinder surrounding the CCP. In the top corner, the argon gas flowing outwards along the top closure goes inwards passing above the internal vessel top. The whirlpool pushes the water pulled along the internal vessel inside the spaces between the neutron shielding and the internal vessel base. In the channel limited by the two vessels, some of the trapped fluid is sent up over the internal vessel top and the rest of the fluid is sent down along the main vessel.

2.4 Deformed shape

The deformed shape of the mesh and the structure deformation are displayed versus time on the figures 8 and 9. The first structures to deform are the neutron shielding and the in-pile plate of the Core Cover Plug. In fact, as they are the structures closest to the explosive charge, they are the first ones to be impacted by the shock wave. We also observe at 0.2 ms a buckling of the lower part of the CCP external cylinder and of the two CCP vertical cylinders representing the pipes, as well as the slight radial displacement of the baffle.

At 0.4 ms, the deformations of the previous quoted structures become more pronounced. We also note a downward deformation of the diagrid and of the main vessel bottom. This deformation is mainly located near the symmetry axis. The lower part of the internal vessel begins moving away.

All the CCP horizontal plates move up. The in-pile shell edge deforms more than the central part because of the violent thrust of the water and bubble gas trying to escape by the free channel between the in-pile shell and the neutron shielding. The CCP spacer plates deform more at the level of the internal and intermediate vertical cylinders than at the centre and at the edge. The cylinders are pushed upwards by the shock wave impact on the in-pile shell. As the in-pile shell is not linked to the external cylinder, the upward thrust is exerted locally.

From 0.6 ms, the upper part of the internal vessel starts moving away owing to the water horizontal thrust at that time. The upper torospherical part of the main vessel also begins moving away.

Between 0.8 and 2 ms, we observe a huge distortion of the neutron shielding and of the baffle because of the large flows of the pressurised bubble gas out of the central zone. The neutron shielding top opens completely while the baffle and the lower part of the internal vessel deforms at mid-height. The in-pile shell bends at once at the edge owing to the fluid escaping by the free channel and at the centre because of the vertical fluid thrust.

In the Core Cover Plug, the external cylinder buckles at the level just below the top closure. The spacer plate deformation becomes more regular: the highest upward displacement is now located at the centre and the lowest displacement near the external vessel. The embedment of the spacer plates with the external cylinder induces an extra-rigidity and thus limits the vertical motion of the plates.

The diagrid and the vessel bottom continue moving down. The main vessel goes down more under the diagrid than under the CSS. The base of the upper part of the internal vessel deforms: as the base of the vertical upper part is fixed to the almost horizontal intermediate part, the outwards horizontal displacement of the upper part causes the bending of the base. A lower bulge forms in the upper part of the torospherical main vessel due to the water flows going up along the main vessel and between both vessels. The Core Support Structure does not move laterally because it is supposed rigid.

From 3 to 5 ms, the deformation of the internal structures increases. It seems that the displacement of the neutron shielding, of the baffle and the lower part of the internal vessel are maximum at that time. The deformation of structures in the lower part of the test-facility seems to remain constant: diagrid, core support structure, main vessel bottom. On the contrary, the structures in the upper part of the test-facility suffer large increasing deformations. For instance, the opening of the upper part of the internal vessel increases.

The core cover plug crushes partially against the heat-insulation; the upper spacer plate goes up and compresses the fluid below the lower plate of the heat-insulation. The lower plate representing the heat-insulation starts bending and going up. The upward motion of the CCP pulls the massive structures of the top closure and we observe the constitution of a sort of stair. The small rotating plug, located next to the CCP, goes up more than the large rotating plug. The roof slab just starts moving at 5 ms.

Between 6 and 9 ms, owing to the compression of the argon gas in the top corner at the junction of the top closure with the main vessel and owing to the going down of the gas in the channel between the two vessels, an upper bulge forms in the upper part of the vessel near the roof. The upper part of the main vessel moves away, what extends the rubber-ring band joining the roof base to the main vessel. Progressively, the upper bulge progresses downward in relation with the downward flow of the pressurised argon and water coming from the roof. At 9 ms, the upper bulge extends from the junction with the roof to the level of the internal vessel intermediate part.

The upward thrust of water and of the bubble gas on the top closure leads to an important deformation of the set of structures composing the top closure. As the shells joining the different parts of the closure do not resist so much as the massive structures, a deformation in stairs appears clearly. The rotating plugs keep their original shape whereas the joining rings are completely out of shape. The roof slab deforms at the level of the two pieces of different thickness. The thicker piece rotates and moves more than the thiner one as this last one is tied up to the hanging device. This device, whose bottom extremity is locked, rotates to allow the going up of the roof slab.

In the core cover plug, as the fluid flows change direction and orient downwards, the lower spacer plate and the in-pile shell come closer at the centre and at the edge. The internal and intermediate cylinders succeed in maintaining a certain distance between both plates at mid-radius of the CCP.

From 10 to 17 ms, the upper bulge takes a pointed shape just above the level of the channel between both vessels. The bulge reaches a maximum extension at 13 ms. The deformation of the internal structures slightly decreases in the central area of the mock-up: the neutron shielding, the baffle and the internal vessel lower part move away because the whirlpool formation pushes fluids in the spaces between these structures.

As the pressurised fluid in the channel between the vessels goes down, the top closure moves slightly back downwards and the hanging device stops rotating and turns back. In the CCP, the depressurisation enables a decompression of the global structure set and a moving apart of the spacer plates. The upper spacer plate moves away from the heat-insulation and the lower spacer plate moves away from the in-pile shell except at the edge.

2.5 Radial displacements of the structures

The figure 10 shows the radial displacements of the structures. The first displacements appear in the lower part of the neutron shielding and in the baffle at 0.24 ms: both structures move away under the impact of the shock wave.

At 0.6 ms, the whole shielding is moving away. The radial displacement increases in the baffle. The lower part of the internal vessel starts going away because the water is propelled horizontally against the structure by the shock wave. On the one hand, we note a slight outward displacement of the upper part of the internal vessel and of the main vessel a little above mid-height because of the water impacting both structures perpendicularly.

On the other hand, the main vessel top moves slightly inwards near the fixing with the roof because the top closure starts going up and rotating under the impact of the upward directed water. As the massive roof slab is much more rigid than the vessel shell, the roof pulls the vessel in its rotation what explains this inward motion.

In the Core Cover Plug, the edges of the spacer plates in contact with the external cylinder move slightly inwards. When the in-pile shell is pushed up by the high pressure bubble in the central area, that produces a local upward motion of the spacer plates at the intersection with the internal and intermediate cylinders. The upward motion of the central part of the spacer plates pulls inwards the extremities of the spacer plates which cannot follow the upward motion due to the rigid link with the external cylinder.

From 1 to 1.5 ms, the previous radial displacements become more marked. In the CCP, due to the upward motion of the inner and intermediate spacer plates, the cylinders are shifted slightly inwards. The external cylinder surrounding the CCP bends at its top extremity because of the compression of the water propelled up against the heat-insulation. As the heat-insulation lower plate is more rigid than the external cylinder, the water thrust induces the cylinder bending rather than the heat-insulation bending.

An inward movement is detected in the main vessel at the junction with the collar supporting the core support structure. The downward bending of the main vessel bottom only under the diagrid at 1 ms induces a local extension of the vessel which pulls down and slightly inwards the vessel located under the CSS. At 1.5 ms, the inward displacement has almost desappeared because the water moves along the vessel towards the collar. The consequence is that the vessel bottom deformation becomes more regular and the vessel bending is only vertical.

At 2 ms, the neutron shielding, the baffle and the internal vessel lower part reach respectively a maximum radial displacement of 60 mm at the top, 45 mm half-way up and 25 mm half-way up. The main vessel continues moving away and reaches a maximum displacement of 15 mm just below the channel between both vessels. The CCP external cylinder bulge under the heat-insulation is still present.

We observe inwards displacements:
- at the main vessel top and the extremity of the CCP spacer plates for the same reasons as before,
- in the intermediate part of the internal vessel because the bubble gas going out from the central zone hurls water against and along the internal vessel intermediate part, causes an outward bending of the upper part of the vessel and also an upward bending of the intermediate part of the vessel which has as a consequence a small inward shifting of the structure,
- in the main vessel above the connection with the collar because the downward displacement of the vessel bottom under the diagrid and the CSS (caused by the downward water thrust in that closed area) also pulls down the main vessel torospherical part above the collar: the vessel looses partially its rounded shape owing to the downward extension.

At 3 and 4 ms, we observe globally the same radial displacements. In the CCP, the value and the location of the displacements remain identical as previously. In the main vessel, the inwards displacement above the collar connection grows, the outwards displacement at mid-height does not evolve and the inwards displacement at the top decreases.

The going out of a large quantity of bubble gas out of the central zone does not change the neutron shielding opening which was already maximum. As the gas is hurled against the internal vessel, it flattens the round corner joining the lower and intermediate parts of the internal vessel. Therefore we observe an outward displacement of the internal vessel intermediate part next to the corner.

The baffle top turns slightly back towards the symmetry axis. As the whipping of this very flexible shell had already brought closer the extremities of the baffle and neutron shielding, the violent expulsion of the bubble gas tilts a bit more the baffle top. This phenomenon is due to height difference between the tall shielding and the short baffle. Besides, fluid is pushed down between the neutron shielding and the baffle what accentuates the baffle bending at mid-height.

From 5 to 8 ms, the radial displacement of the neutron shielding remains constant. The baffle top opens outwards because the fluid previously pushed between the baffle and the shielding rebounds against the core support structure. By flowing up and going out of the space between both shells, the fluid forces the baffle top to move away.

The radial displacements decrease in the lower and intermediate parts of the internal vessel because the fluid flows change direction. Before, outward directed fluid coming from the mock-up centre impacted the internal vessel from above; now the internal vessel is impacted from below by water inward directed which has rebounded against the main vessel. On the contrary, the internal vessel upper part moves away. It reaches a maximum displacement of about 15 mm at 7 ms. In that area, the fluid is propelled almost horizontally against the internal vessel.

The radial displacements at the extremities of the core cover plug spacer plates and in the main vessel above the collar connection remain constant until the end of the computation.

In the main vessel, the inward displacement at the top desappears because of the important fluid flows along the top closure which pass over the internal vessel top and impacts perpendicularly the main vessel top. From 6 ms, the main vessel top moves outwards because the fluid starts flowing down in the channel between both vessels: an upper bulge creates. As the fluid flows down in the channel, the upper bulge moves down too and extends. Progressively the upper bulge joins the lower bulge at the level of the channel base.

The top closure going up from 5 ms under the thrust of the fluid impacting the whole closure, this upward motion is accompanied by a rotation of the closure around the locked point at the bottom extremity of the hanging device. The rotation induces an inward displacement of the closure, more marked near the external radius than in the centre. That rotation explains the inward displacement recorded at the bottom of the large rotating plug, on the lower half-height of the roof slab and at the top of the hanging device.

Between 9 and 10 ms, we observe a rise of the outwards radial displacements in the main vessel at mid-height of the channel between the vessels and at the top of the baffle. The inwards displacement in the roof slab and the large rotating plug increases too. The displacement of the internal vessel decreases slightly because the fluid flowing in the channel pushes the internal vessel inwards. The displacement of the neutron shielding remains constant.

From 11 to 12 ms, the radial displacements increase at the level of the main vessel upper bulge and the baffle top. They reach respectively a maximum of 35 mm and 25 mm at 12 ms. The inward displacements decrease in the top closure as the closure rotates back: the fluid moves back downwards after having rebounded against the closure. Under the effect of the whirlpool formation, the internal vessel intermediate part bends: near the upper cylinder, the shell moves up and inwards pushed by the fluid coming from the channel and flowing below the plate; near the lower cylinder, the intermediate plate conserves its outwards displacement.

From 13 to 17 ms, the inward radial displacement in the top closure, induced by the closure rotation, decreases in the roof slab. There is no more radial displacement in the large rotating plug and the hanging device. Elsewhere the displacements remain constant.

2.6 Vertical displacements of the structures

The figure 11 presents the vertical displacements of the structures. The first structures to displace vertically are the Core Cover Plug and the diagrid. These structures are the nearest from the central explosive charge. The in-pile shell is pushed up by the explosive pressure while the diagrid moves downwards. The base of the neutron shielding suffers a small downward displacement caused by the radial opening of the structure. At 0.4 ms, we also observe a downward motion of the main vessel bottom just under the diagrid.

At 0.8 ms, the diagrid and the vessel bottom continue going down because of the impact of water hurled downwards by the explosion. Meanwhile, almost all the rest of the main vessel starts moving down because the whole vessel is pulled down by the high thrust on its base. As the vessel top is almost vertically blocked by the embedment of the handling device, the downward deformation is proportional to the distance from the top.

In the CCP, the in-pile shell being pushed up, it drags in its upward motion the internal and intermediate cylinders simulating the pipes and the part of the spacer plates between the symmetry axis and the intermediate plate. The external cylinder does not move as it is not directly linked to the in-pile shell. Due to the radial opening of the lateral structures (neutron shielding, lower part and top of the internal vessel), we also notice a downward displacement of these structures.

From 1.2 to 1.6 ms, the downward deformations increase in the diagrid, the main vessel and the neutron shielding. These deformations extend to the whole Core Support Structure and the collar, the whole upper part of the internal vessel and the majority of the intermediate part of this vessel. As the CSS is attached to the vessel bottom, the accentuation of the downward motion of the vessel causes in turn the downward motion of the attached structures. The only exception concerns the baffle: the water motions in that area involves a rounded deformation and a streching of the shell.

In the CCP, we note an upward motion more important at the centre than near the external cylinder. Because of the upward thrust of the water inside the CCP, the internal and intermediate cylinders stretch and the spacer plates deform more at the centre where they are free to move than at the edge where they are linked to the external cylinder. As the external cylinder buckles just under the top-closure level, we observe a shortening of the cylinder and thus an upward displacement of the structure.

Between 2 and 2.8 ms, the downward displacements of the main vessel, core support structure and collar, diagrid, neutron shielding and lower part of the internal vessel become more pronounced. The diagrid centre and the shielding top reach a maximum displacement of -30 mm downwards at 2.8 ms. The CSS displacement is around -10 mm. The junction of the lower and intermediate parts of the internal vessel suffers a maximum displacement of about - 20 mm.

The whole CCP part plunging inside the fluid goes on moving upwards and the very flexible baffle continues stretching and moving up because of the upwards thrust of the fluid which rebounded against the CSS. Because of the upward motion of the water below the internal vessel intermediate part, this part of the vessel stops moving down.

From 3.2 to 3.6 ms, the deformations of the diagrid, neutron shielding, baffle, CSS and collar remain constant. Owing to the upward fluid flow in the channel between both vessels, the upper part of the internal vessel moves back upwards. In the mock-up centre, the CCP part plunged into the fluid continues going up because of the water flows oriented upwards in the CCP; those flows contribute to push the upper spacer plate as well as the heat-insulation lower plate and to crash the external cylinder bulge due to the buckling against the top closure. At 3.6 ms, the lower plate of the CCP heat-insulation starts going up too.

From 4 to 9 ms, the main vessel bottom and the diagrid stop moving down and move back upwards due to the rebound of the water against the vessel bottom and the reversal of the water flow under the diagrid. In its upward motion, the vessel bottom pulls up the rest of the main vessel, the collar and the CSS, as well as the neutron shielding, the baffle and the internal vessel lower part. Due to the downward flow of fluid coming from the top closure and passing over the internal vessel to go inside the channel between the two vessels, the upper part of the internal vessel moves down (buckling and bending of the structure).

The CCP continues moving up towards the heat-insulation; the external cylinder upper part is partially crashed against the top closure. The reason of this upward motion is that the in-pile shell is still pushed up by the bubble gas expanding from the central zone and that the fluid inside the CCP continues to be hurled upwards and to impact the upper spacer plate. The consequence of these phenomena is that the in-pile shell, the internal cylinder and the central part of the spacer plates reach a maximum displacement of 100 mm at 9 ms.

The water and argon vertical thrust all along the CCP heat-insulation and the top closure induces a rotation of the upper and massive part of the mock-up around the fixed point at the extremity of the hanging device. Therefore we observe an upward displacement of the top closure and the heat-insulation, more important near the symmetry axis than near the closure edge. The deformation occurs by stairs: the joining rings being much flexible than the massive structures, the pieces shift up mainly at the ring level. The maximum displacement is observed in the lower heat-insulation plate; at 9 ms, it reaches 30 mm in that plate and about 20 mm in the small rotating plug and the other plates simulating the heat-insulation.

From 10 to 12 ms, the main vessel, the diagrid, the neutron shielding and the internal vessel lower part keep on moving back upwards because the water flows slow down below the diagrid. The baffle top continues moving up and deforms more or less like rubber under the contradictory fluid flows due to the whirlpool formation and the upward flow between the neutron shielding and the internal vessel lower after the rebound of the fluid against the CSS.

In spite of the downward flows in the channel between both vessels, the intermediate and upper parts of the internal vessel move up because of the upward thrust of the water flowing below the internal vessel. The formation of the upper bulge contributes to pull up the main vessel part located between the collar junction and the bottom of the channel between the vessels.

In the CCP, the fluid flows reverse and orient downwards, so that they push down the spacer plates. Consequently the whole CCP moves back down. With the formation of the whirlpool just above the baffle, the fluid is attracted from below the top closure; the top closure compression stops and the structures move back.

From 14 to 17 ms, the whirlpool pushes violently the fluid inside the central area. This fluid impacts the diagrid which moves down again. Simultaneously, the neutron shielding top and the in-pile shell edge move away too. The impact against the diagrid causes a downward motion of the water below the diagrid. When this water impacts the vessel bottom, the main vessel bottom goes down once again. It pulls down the rest of the main vessel and the structure set attached to it.

The fluid inside the CCP rebounds against the spacer plates and goes up a second time. In parallel, the fluid propelled inside the central area pushes upwards the CCP base. Consequently the whole CCP (spacer plates, cylinders and heat-insulation) moves up another time. The pressurised fluid escapes by the perforated part of the external cylinder below the top closure and spreads under the top closure which moves up again.

2.7 Von Mises stresses in the structures

The figure 12 shows the stresses in the external and internal structures. The first stresses appear in the neutron shielding, the in-pile shell and the bottom of the CCP internal and intermediate cylinders. They correspond to the impact of the pressure wave on the structures limiting the central area.

At 0.2 ms, the baffle and the internal vessel lower part are submitted to stresses because the pressure wave has impacted these structures. As the pressurised zone goes until the base of the CCP heat-insulation, the complete part of the CCP plunging into the fluid is submitted to stresses, with local higher values at the junctions between plates and cylinders. As the CCP external cylinder is rigidly linked to the plates simulating the heat-insulation, the cylinder lower part transfers part of the stresses to the cylinder upper part, which in turn compresses the edge of the plates in contact with the cylinder.

At 0.3 ms, the new zones under stress are the main vessel bottom and the intermediate part of the internal vessel owing to the shock wave progression towards the vessel. The stresses decrease in the CCP internal cylinder and at the centre of the spacer plates because of the pressure decrease in that area. The ring joining the upper heat-insulation plate to the top of the small rotating plug is also submitted to stresses due to the upwards sliding of the CCP relatively to the massive rotating plug.

From 0.4 to 0.5 ms, the stress level goes on increasing in the neutron shielding, the baffle, the internal vessel, the collar and the main vessel from the collar attachment to the roof junction. This period corresponds to an important speed of about 20 m/s of the water hurled against the structures in that area. After having reached a maximum stress of 600 MPa at the main vessel bottom at 0.4 ms, the stress level decreases due to the depressurisation of the area below the diagrid.

High stress spots appear in the main vessel at the attachment of collar and at the connection between the torospherical and the cylindrical pieces of the vessel (different thickness of the vessel in both parts). In the CCP, the stresses rise at the junctions between the shells and the cylinders because the fluid going up pushes the plates and deforms them. On the contrary, the stresses decrease in the cylinders between both upper spacer plates: the fluid flows along the internal and intermediate cylinders which are not coupled to the structures.

Due to the upward directed thrust of the water impacting the top closure in the area around the CCP, the stresses increase in the ring joining both rotating plugs. This stress concentration in the rings is the reason of the top closure deformation in stair shape. As the massive part of the closure is very strong and rigid, it cannot deform and the stresses do not increase. The core support structure being very thick, the stress level remains very low in this structure. The stresses remain limited in the diagrid support because the constitutive law of this structure presents a very low plastic threshold.

From 0.6 to 1.2 ms, the stresses increase in the neutron shielding and the baffle because, at that time, the high pressure bubble gas starts escaping from the central zone and thus exerts a thrust on the neighbouring structures. The stresses remain unchanged in the internal vessel lower part but decrease in the intermediate part and at the top of the upper part due to the pressure decrease in that area.

The stresses raise in the main vessel bottom and the collar because the water is hurled continuously against the vessel bottom since 0.3 ms. A maximum stress level of 600 MPa is reached at the vessel bottom at 1.2 ms. A high stress spot appears at the junction between the vessel and the collar because the connection of the main vessel with the rigid Core Support Structure prevents a free deformation of the vessel under the water thrust.

In the torospherical part of the main vessel located above the collar, the stresses raise at 0.8 ms because of the arrival of a pressure wave hitting the vessel and rebounding on it. Then the stresses go down again when the pressure wave goes away from the vessel. In the vertical part of the main vessel, the stresses decrease slightly because the fluid speeds are much lower in the channel than previously.

In the CCP, the stresses fall due to the local pressure fall in the surrounding fluid. Owing to the high thrust of the fluid hurled against the top closure, the joining rings suffer a regular stress increase. Besides the hanging device is also submitted to stresses: the upward thrust against the top closure tends to make rotate the closure around the fixed low extremity of the hanging device.

Until 1.6 ms, the stresses increase in the neutron shielding: they reach a maximum of 650 MPa at the top of the shell at 1.6 ms. The stresses continue raising in the baffle at mid-height and remain constant in the lower part of the internal vessel. Between 1.6 and 2 ms, the stresses decrease in the three structures as the pressure in the central area and between the vertical shells decreases at that time.

From 1.2 to 2 ms, the location of the maximum stress in the main vessel bottom moves towards the collar, following on that way, the fluid motion along the vessel towards the collar. The high stress spot at the collar junction persists. The stress in the rest of the main vessel evolves according to the fluid pressure evolution. The stresses decrease at 1.6 ms when the pressure wave goes away from the main vessel towards the internal vessel. At 2 ms, the stresses increase again due to the going back of the pressure wave.

In the internal vessel intermediate part, the stresses raise because this vessel part is submitted to the rebounds of the pressure wave oscillating between both vessels. On the contrary, the stresses decrease in the upper vertical part of the internal vessel due to the low pressure in that area at that time.

In the CCP, the stresses remain limited in the internal and intermediate cylinders. The stresses fall in the spacer plates and even in the in-pile shell due to the low local pressure at that time. However, we can observe the presence of stress concentration at the junctions of the three spacer plates with the external cylinder. These local high stress spots reach a maximum value of 750 MPa at 1.6 ms; they are caused by the deformation of the spacer plates whose upward motion is limited by the junction with the external cylinder.

In the lower heat-insulation plate, the stresses raise because of the impact of the fluid inside the CCP which is propelled upwards against the upper CCP part limiting the fluid zone. Their maximum value is obtained at 2 ms and worths 200 MPa. Simultaneously, the external cylinder zone just below the heat-insulation is submitted to a high stress increase (500 MPa) in relation with the local buckling of the cylinder.

In the top closure, the stresses go on increasing in the two joining rings between the rotating plugs and the roof. The stresses are maximum at 2 ms; their values are 500 MPa between the rotating plugs and 800 MPa between the large plug and the roof. This increase comes from the fluid motion under the top closure towards the closure outer limit. The stresses also increase in the hanging device and in the rubber band joining the roof to the main vessel. All these stress rises are due to the top closure rotation around the low extremity of the hanging device.

Between 3 and 5 ms, the stress level is much lower in the neutron shielding and in the in-pile shell than at 2 ms, as the free space between both structures is considerably enlarged. As the CCP external cylinder reaches its maximum buckled position at 3 ms and the shielding top its maximum radial displacement at 2 ms, the space between both structures is maximum since 3 ms and it remains constant until 10 ms.

In the baffle, a maximum stress level of 550 MPa is reached at 3 ms at the shell top. At that instant, the panache of high pressure bubble gas escaping from the central area hits head-on the baffle top with high velocities. Between 4 and 5 ms, the stresses decrease in the baffle in relation with the fluid speed decrease in that area.

In the internal vessel, the stresses fall in the lower part and raise in the intermediate and upper parts because the pressurised area is located in the upper part of the mock-up between 3 to 5 ms.

In the main vessel bottom, the stress level and the stress location are linked to the pressure wave rebounds and the pressure damping. When the pressure wave impacts the collar at 3 ms, a maximum stress of 600 MPa is located in the collar vicinity. As the pressure wave is reflected towards the symmetry axis, the local maximum stress goes back towards the axis too. The collar being flexible, it absorbs partially the pressure impact by its deformation and the reflected wave is lower than the incident one. Consequently, the stress level is lower in the main vessel at 4 ms than at 3 ms. The port under the diagrid being larger than the one under the CSS, the pressure and thus the stresses become even lower at 5 ms.

In the torospherical part of the main vessel located above the collar, the stresses go on increasing until 3 ms because the impact of the pressure wave hitting the collar is partially transmitted to the other side of the vessel. Then the stresses decrease regularly as the water pressure remains low in the area located between the CSS and the main vessel.

In the cylindrical part of the main vessel, the stresses decrease first at 3 ms before increasing again. Indeed the fluid is propelled upwards against the top closure at 3 ms whereas it flows along the closure towards the main vessel since 4 ms.

In the CCP, the stress level is rather weak, except at the connections of the spacer plates and the lower heat-insulation plate with the external cylinder. At 3 ms, the important upward fluid flow goes on bending the spacer plates what explains the presence of the high stress spots at the edge of the plates. As the buckling of the external cylinder ends at 3 ms, the stress level increases too at the junction with the heat-insulation.

At 4 ms, on the one hand, the upward fluid flow slows down so that the stresses decrease in the spacer plates and at their junction with the external cylinder. On the other hand, the fluid accumulation under the lower heat-insulation plate, simultaneously with the arrival of the pressure wave which rebounded on the internal vessel, leads to the bending of the heat-insulation plate. This plate is submitted to homogeneous stresses all along the plate, with a stress concentration at the connection with the cylinder.

At 5 ms, as the fluid goes out laterally from the CCP, the stresses decrease at once in the heat-insulation and in the external cylinder top. However, stress spots at the base of the external cylinder are the consequence of the expansion of the high pressure bubble gas out of the central zone.

In the top closure, the stresses increase in the upper ring joining the CCP to the small plug due to the vertical thrust on the heat-insulation plate. The stresses decrease in the rings between both rotating plugs and between the large plug and the roof because the pressurised fluid flows towards the main vessel. The stress level remains constant in the hanging device as the fluid flows under the closure are no more oriented upwards. The stresses raise in the rubber band joining the roof to the main vessel which extends because of the formation of the main vessel upper bulge due to the fluid flows in the channel between both vessels.

From 6 to 17 ms, the stresses decrease in the main vessel bottom because of the pressure fall in the area between the diagrid and the main vessel. The stress concentration at the junction with the collar alternately increases and decreases according to the rebounds of the water between the main and internal vessels.

The stresses also decrease in the part of the main vessel located above the collar due to the progressive pressure decrease in the area between both vessels. However, the cylindrical upper part of the main vessel continues to suffer stresses up to 600 MPa at the level of the channel; as the fluid coming from the roof moves down in the channel, the location of the maximum stress follows the fluid motion. The maximum stress is observed at the location of the upper vessel bulge.

In the internal vessel, the stresses decrease: with the formation of the whirlpool, the fluid is attracted from the vicinity of the internal vessel towards the baffle. Consequently the pressure exerted on the vessel decreases.

The baffle is submitted to high stresses (up to 600 MPa) in the whole shell at 6 ms. At that time, the baffle is pushed away at once by the bubble gas going out from the central zone and by the mixture of bubble gas and water which rebounds on the CSS after having been projected in the space between the shielding and the baffle. From 8 to 10 ms, the stresses decrease in the baffle because the fluid is still oriented upwards and that the baffle does not move away more. At 12 ms, the stresses increase at the base of the baffle because the fluid orients perpendicularly to the shell in a local zone. From 14 to 17 ms, the fluid moves down again in the space between the shielding and the baffle and thus causes a stress increase in the rest of the baffle.

From 4 to 17 ms, the small whirlpool in the internal zone exerts a thrust against the neutron shielding at mid-height, what is the reason of the stresses observed at mid-height of the shielding. The level of the stress depends on the orientation of the fluid impacting the shell.

In the CCP, the stresses remain very weak in the internal and intermediate cylinders because there is no fluid-structure coupling with these cylinders. The in-pile shell and the spacer plates remain submitted to more or less constant stresses linked to the thrust of the fluid whirling in the central zone. The level of the stress concentration at the junctions of the spacer plates with the external cylinder is linked at once to the orientation of the fluid flow inside the plug and to the pressure exerted on the cylinder by the large whirlpool.

In parallel with the vertical displacement in stairs of the top closure, we observe a stress increase in the joining rings and the hanging device between 6 and 10 ms. The stress level decreases from 12 ms simultaneously with the going back of the closure due to the pressure decrease under the top closure. The highest stresses (900 MPa) are observed in the ring between the roof and the large rotating plug: as the roof slab is larger than the three plugs, its deformation is more limited than the one of the plugs and thus the strain of the nearest ring is higher.

The stress level remains very low in the rigid structures (massive structures of the top closure, thick shell such as the CSS). In the diagrid support, the stresses remain limited because the structure becomes almost immediately plastic and suffers large deformations compared to the stress level.

2.8 Plastic strains of the structures

The figure 13 shows the plastic strains of the structures versus time. At 0.2 ms, the whole neutron shielding has become plastic and the baffle starts becoming plastic. The plastic strains are due to the impact of the shock wave on these structures from respectively 0.06 and 0.1 ms.

At 0.3 ms, the plastic strains increase in both structures. The diagrid support edge near the CSS suffers plastic strains because of the impact of the shock wave on the structure since 0.1 ms. As the structure is relatively thick, its deformation is much smaller than the ones of the shielding. The in-pile shell, the lower and upper spacer plates, as well as the lower part of the external CCP cylinder show small plastic strains. They are due to upward rising of the CCP pushed up by the shock wave.

From 0.4 to 0.8 ms, the strain level raises in the previous structures because they are included in the pressurised area. In addition, the part of the main vessel bottom under the diagrid becomes plastic because the shock wave hits it at 0.26 ms and since this instant the water under the diagrid is propelled towards the vessel.

The lower part of the internal vessel suffers plastic strains from 0.4 ms: the shell is impacted by the shock wave from 0.14 ms. The whole cylindrical part of the main vessel become plastic from 0.6 ms due to the impact of the shock wave since 0.34 ms. In the CCP, the junction of the spacer plates and the external cylinder suffer plastic strains since 0.6 ms because of the violent thrust of the fluid on the spacer plates: the plates present a high bending from 0.8 ms.

Between 1 and 1.2 ms, the plastic level increases strongly in the neutron shielding, the baffle and the diagrid support. The strains increase too in the lower part of the internal vessel, in the CCP, in the bottom and the cylindrical part of the main vessel. Plastic strains appear in the CCP external cylinder below the heat-insulation: that corresponds to the buckling of the shell. The ring joining the two rotating plugs becomes plastic due to the high fluid thrust under the top closure.

Between 1.6 and 5 ms, the strain level raises mainly in the neutron shielding, the baffle, the ring between both rotating plugs and the junction of the CCP external cylinder with the heat-insulation plate. In the shielding, the strain level reaches a maximum of 40 % at 1.6 ms at the shell top. In the baffle, the maximum level is obtained at 2.2 ms at mid-height. The strains increase more moderately in the diagrid, the internal vessel lower part, the main vessel bottom and upper part. A maximum plastic strain level of 8 % is reached at the centre of the diagrid support and in the whole lower part of the internal vessel respectively at 1.6 ms and 4 ms.

From 1.6 ms, plastic strains appear in the ring joining the large plug to the roof due to the motion of the pressurised fluid from the CCP towards the main vessel. The heat-insulation plate of the CCP becomes plastic from 3 ms at the junction with the cylinder. Its maximum strain level is reached at 5 ms. At 4 ms, the centre of the heat-insulation plate also presents some plastic strains due to the high thrust exerted by the fluid hurled and compressed under the shell.

From 6 to 17 ms, the plastic strains remain constant in the shielding, the baffle, the diagrid, the main vessel bottom and the majority of the CCP. On the contrary, they increase in the internal vessel at the junction between the lower and intermediate parts because the whirlpool causes a bending of the intermediate part by pulling the fluid all along the vessel intermediate part.

The plastic strains also increase in the main vessel cylindrical part because of the formation of the upper vessel bulge: the fluid flowing down in the channel between both vessels deforms the main vessel. In relation with the fluid flowing from the roof to the base of the channel, the plastic strains extend from the top to the bottom of the cylindrical part of the main vessel. A uniform plastic strain of about 8 % is reached in the main vessel at the height of the channel.

In the two rings joining the rotating plugs and the roof slab, the plastic level increases until 14 ms because of the fluid flows below the top closure, generated by the whirlpool. Maximum plastic strains of 14 % and 20 % are observed at 14 ms, respectively in the ring between the small and large rotating plugs and between the large plug and the roof slab.

3 CONCLUSION

In that paper, we present a computation of a Hypothetical Core Disruptive Accident in the MARS test-facility which is a small scale replica of a Fast Breeder Reactor. This mock-up contains all the internal structures of the reactor block. The fluids intervening in the real accident were replaced by water, argon and an explosive charge in the experiment.

In the numerical model, the majority of the structures are represented by shells or massive structures. However, the internal structures of complex geometry in the area of the internal vessels are simply taken into account by a pressure loss. The internal fluids are described by the specific CDA constitutive law implemented on purpose in the CASTEM-PLEXUS code for computing this kind of explosion.

The explosive wave propagates from the centre of the mock-up towards the main vessel and the top closure. The passing of the pressure wave loads and deforms the internal structures and then the external ones. The structures most in demand are the neutron shielding and the core cover plug because of their proximity with the pressurised area.

The high pressure gas bubble in the central part of the mock-up expands in the rest of the test-facility, thus pushing away the top of the neutron shielding and the in-pile shell. The argon layer under the top closure is pushed below the roof and in the channel between the internal and main vessels. A bulge forms in the upper part of the main vessel during the passing of the pressurised fluid in the channel.

During the explosion, the water contained into the mock-up is accelerated and hurled against the structures. In particular, the water impacts perpendicularly the main vessel and the top closure. The water thrust leads to a large deformation of the main vessel bottom. The fluid impacting the top closure causes a deformation in stairs (more important at the centre than at the edge) linked to the lower rigidity of the joining rings linking the massive slabs (plugs and roof).

In order to predict the influence of the peripheral structures (pumps, heat exchangers) acting as porous barriers and consequently having a protective effect on the containment by absorbing energy and slowing down the fluid impacting the containment, we developped in CASTEM-PLEXUS a new HCDA model taking into account the presence of the internal structures (without meshing them) by means of an equivalent porosity method (Robbe[b], 1999) (Robbe[c], 1999). This model has been applied to predict the MARS test.

REFERENCES

Acker, D., Benuzzi, A., Yerkess, A., Louvet, J., August 1981. MARA 01/02 - Experimental validation of the SEURBNUK and SIRIUS containment codes, Proc. 6th Int. Conf. on Structural Mechanics In Reactor Technology, Section E 3/6, Paris, France.

Albertini, C., et al. The JRC-COVA programme : Final Report. Commission of the European Communities, Report EUR 8705, 1983. Nuclear Science and Technology, 1984, pp. 1-182.

Benuzzi, A., 1987. Comparison of different LMFBR primary containment codes applied to a benchmark problem, Nuclear Engineering and Design 100, 239-249.

Blanchet, Y., Obry, P., Louvet, J., August 1981. Treatment of fluid-structure interaction with the SIRIUS computer code, Proc. 6th Int. Conf. on Structural Mechanics In Reactor Technology, Section B 8/8, Paris, France.

Bour, C., Spérandio, M., Louvet, J., Rieg, C., August 1989. LMFBR's core disruptive accident. Mechanical study of the reactor block, Proc. 10th Int. Conf. on Structural Mechanics In Reactor Technology, Vol. E, Anaheim, pp. 281-287.

Cameron, I.G., Hankin, B.C., Warham, A.G.P., Benuzzi, A., Yerkess, A., August 1977. The computer code SEURBNUK-2 for fast reactor explosion containment safety studies, Proc. 4th Int. Conf. on Structural Mechanics In Reactor Technology, Section B 2/1, San Francisco, USA.

Cariou, Y., Spérandio, M., Lepareux, M., Christodoulou, K., August 1993. LMFBR's whole core accident. Validation of the PLEXUS code by comparison with MARA tests, Proc. 12th Int. Conf. on Structural Mechanics In Reactor Technology, Section E 7/4, Stuttgart, Germany.

Cariou[a], Y., Pirus, J.P., Avallet, C., August 1997. LMR large accident analysis method, Proc. 14th Int. Conf. on Structural Mechanics In Reactor Technology, Section P 3/7, Lyon, France, pp. 395-402.

Cariou[b], Y., Lepareux, M., Noé, H., August 1997. LMR's whole core accident. Validation of the PLEXUS code by comparison with MARS test, Proc. 14th Int. Conf. on Structural Mechanics In Reactor Technology, Section P 2/6, Lyon, France, pp. 339-346.

Casadei, F., Daneri, A., Toselli, G., August 1989. Use of PLEXUS as a LMFBR primary containment code for the CONT benchmark problem, Proc. 10th Int. Conf. on Structural Mechanics In Reactor Technology, Section E 13/1, Anaheim, pp. 299-304.

Chang, Y.W., Gvildys, J., Fistedis, S.H., 1974. Analysis of the primary containment response using a hydrodynamic-elastic-plastic computer code, Nuclear Engineering and Design 27, 155-175.

Chang, Y.W., 1977. Application of containment codes to LMFBRs in the United States, Nuclear Engineering and Design 42, 53-67.

Chavant, C., Hoffmann, A., Verpeaux, P., Dubois, J., 1979. Plexus: A general computer code for explicit Lagrangian computation, Proc. 5th Int. Conf. on Structural Integrity In Reactor Technology, Section B 2/8, Berlin, Germany.

Cigarini, M., Daneri, A., Toselli, G., August 1983. Applications of ASTARTE-4 code to explosive models with complex internal structure using the rezoning facility, Proc. 7th Int. Conf. on Structural Mechanics In Reactor Technology, Section B 9/3, Chicago, USA.

Cowler, M.S., Hancock, S.L., 1979. Dynamic fluid-structure analysis of shells using the PISCES 2 DELK computer code, Proc. 5th Int. Conf. on Structural Mechanics In Reactor Technology, Section B 1/6, Berlin, Germany.

Daneri, A., Toselli, G., Trombetti, T., Blanchet, Y., Louvet, J., Obry, P, August 1981. Influence of the representation models of the stress-strain law on the LMFBR structures in an HCDA, Proc. 6th Int. Conf. on Structural Integrity In Reactor Technology,

Section E 4/4, Paris, France.
David, F., 1978. Etude d'une composition explosive flegmatisée. Applications à la déformation d'une cuve, Proc. Symposium sur les hautes pressions dynamiques, Paris, France.
Falgayrettes, M., Fiche, C., Granet, P., Hamon, P., Barrau, P., Magnon, B., Jalouneix, J., Nédélec, M., 1983. Response of a 1/20 scale mock-up of the Superphenix breeder reactor to an HCDA loading simulation, Proc. 7th Int. Conf. on Structural Mechanics In Reactor Technology, Section E 4/1, Chicago, USA, pp. 157-166.
Fiche, C., Louvet, J., Smith, B.L., Zucchini, A., August 1985. Theoretical experimental study of flexible roof effects in an HCDA's simulation, Proc. 8th Int. Conf. on Structural Integrity In Reactor Technology, Section E 4/5, Brussels, Belgium, pp. 139-144.
Graveleau, J.L., Louvet, P., August 1979. Calculation of fluid-structure interaction for reactor safety with the CASSIOPEE code, Proc. 5th Int. Conf. on Structural Mechanics In Reactor Technology, Section B 1/7, Berlin, Germany.
Hoffmann, A., Lepareux, M., Schwab, B., Bung, H., 1984. Plexus - A general computer program for fast dynamic analysis, Proc. Conference on Structural Analysis and Design on Nuclear Power Plant, Porto Alegre, Brazil.
Holtbecker, H., 1977. Testing philosophy and simulation techniques, Nuclear Engineering and Design 42, 75-87.
Hoskin, N.E., Lancefield, M.J., 1978. The COVA programme for the validation of computer codes for fast reactor containment studies, Nuclear Engineering and Design 46, 17-46.
Idel'Cik, I.E., 1986. Memento des pertes de charge. Coefficients de pertes de charge singulières et de pertes de charge par frottement, Collection de la Direction des Etudes et Recherche d'EDF, Eyrolles, Paris, France, p. 362.
Kendall, K.C., Benuzzi, A., 1980. The COVA programme : Validation of the fast reactor containment code SEURBNUK, Nuclear Engineering and Design 57, 79-105.
Kendall, K.C., Adnams, D.J., 1986. Experiments to validate structural dynamics code used in fast reactor safety assessment, Science and Technology of Fast Reactor Safety, Vol. 2, British Nuclear Energy Society, London, England.
Lepareux, M., Bung, H., Combescure, A., Aguilar, J., August 1991. Analysis of a CDA in a LMFBR with a multiphasic and multicomponent behaviour law, Proc. 11th Int. Conf. on Structural Mechanics In Reactor Integrity, Section E 13/1, Tokyo, Japan, pp. 371-376.
Lepareux, M., Bung, H., Combescure, A., Aguilar, J., Flobert, J.F., August 1993. Analysis of an HCDA in a fast reactor with a multiphase and multicomponent behavior law, Proc. 12th Int. Conf. on Structural Mechanics In Reactor Integrity, Section E 7/2, Stuttgart, Germany, pp. 197-202.
Louvet, J., Hamon, P., Smith, B.L., Zucchini, A., August 1987. MARA 10: an integral model experiment in support of LMFBR containment analysis, Proc. 9th Int. Conf. on Structural Mechanics In Reactor Integrity, Section E, Lausanne, Switzerland, pp. 331-337.
Louvet., J., August 1989. Containment response to a core energy release. Main experimental and theorical issues - Future trends, Proc. 10th Int. Conf. on Structural Mechanics In Reactor Integrity, Vol. E, Anaheim, pp. 305-310.
NERSA, 1987. The Creys-Malville power plant, Electricité de France, Direction de l'équipement, Région d'équipement Alpes-Lyon, France.
Robbe, M.F., Lepareux, M., Bung, H. Plexus - Notice théorique, CEA report DMT/94-490, 1994.
Robbe[a], M.F., Galon, P., Yuritzinn, T., November 1999. Castem-Plexus: Un logiciel de dynamique rapide pour évaluer l'intégrité des structures en cas d'accident, Proc. 4th Conf. INSTRUC, Courbevoie, France.
Robbe[b], M.F., August 1999. A porosity method to model the internal structures of a reactor vessel, Proc. 15th Int. Conf. on Structural Mechanics In Reactor Technology, Vol. B, Seoul, Korea.
Robbe[c], M.F., Bliard, F., April 1999. A porosity model to represent the influence of structures on a fluid flow. Application to a hypothetical core disruptive accident, Proc. 7th Int. Conf. On Nuclear Engineering, paper 7819, Tokyo, Japan.
Sidoli, J.E.A., Kendall, K.C. The WINCON programme - Validation of the fast reactor primary containment codes. Proc. INE Int. Conf. On Nuclear Containment, Cambridge, England, April 1987. Nuclear Containment Structures, D.G. Walton, Cambridge University Press, 1988.
Smith, B.L., Yerkess, A., Adamson, J., August 1983. Status of coupled fluid-structure dynamics code SEURBNUK, Proc. 7th Int. Conf. on Structural Mechanics In Reactor Technology, Section B 9/1, Chicago, USA.
Smith, B.L., Fiche, C., Louvet, J., Zucchini, A., August 1985. A code comparison exercise based on the LMFBR containment experiment MARA-04. Proc. 8th Int. Conf. on Structural Mechanics In Reactor Technology, Section E 4/7, Brussels, Belgium, pp. 151-157.
Smith B.L., Yerkess, A., Washby, V., August 1987. The computer code SEURBNUK-EURDYN: First release version, Proc. 9th Int. Conf. on Structural Mechanics In Reactor Technology, Lausanne, Switzerland.
Stiévenart, M., Bouffioux, P., Eglème, M., Fabry, J.P., Lamotte, H. August 1975. Analysis of LMFBR explosion model experiments by means of the Surboum-II code, Proc. 3rd Int. Conf. on Structural Mechanics In Reactor Technology, Section E 3/5, London, England.
Wenger, H.U., Smith, B.L., 1987. On the origin of the discrepancies between theory and experiment in the COVA series, Proc. 9th Int. Conf. on Structural Mechanics In Reactor Technology, Vol. E, Lausanne, Switzerland, pp. 339-344.
West, P.H., Hoskin, N.E. APRICOT - Phase 3. Suggested simple test problems for examination of thin shell modelling and fluid structure coupling, Aldermaston report AWRE/44/92/16, 1980.

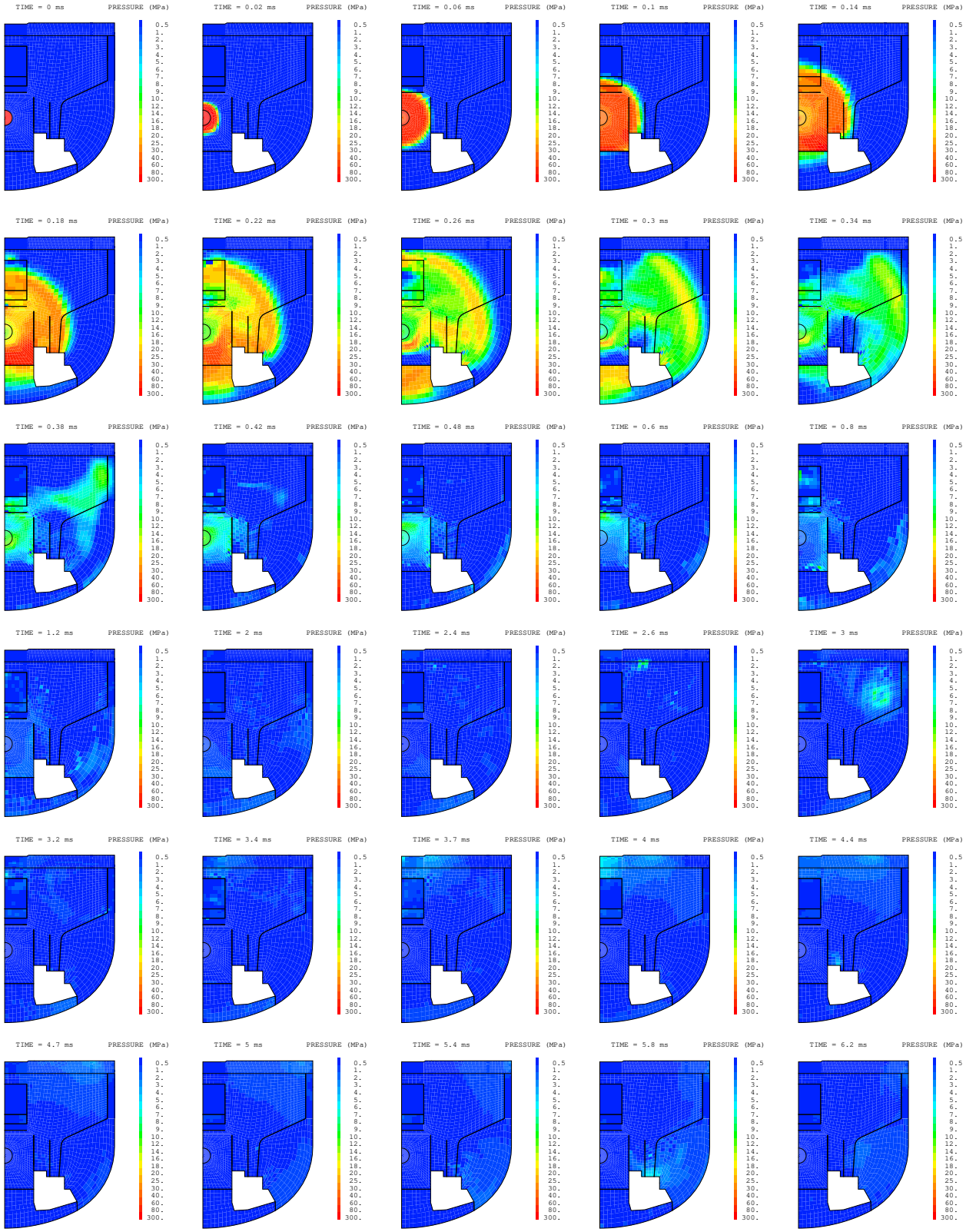

Fig. 2: Pressure

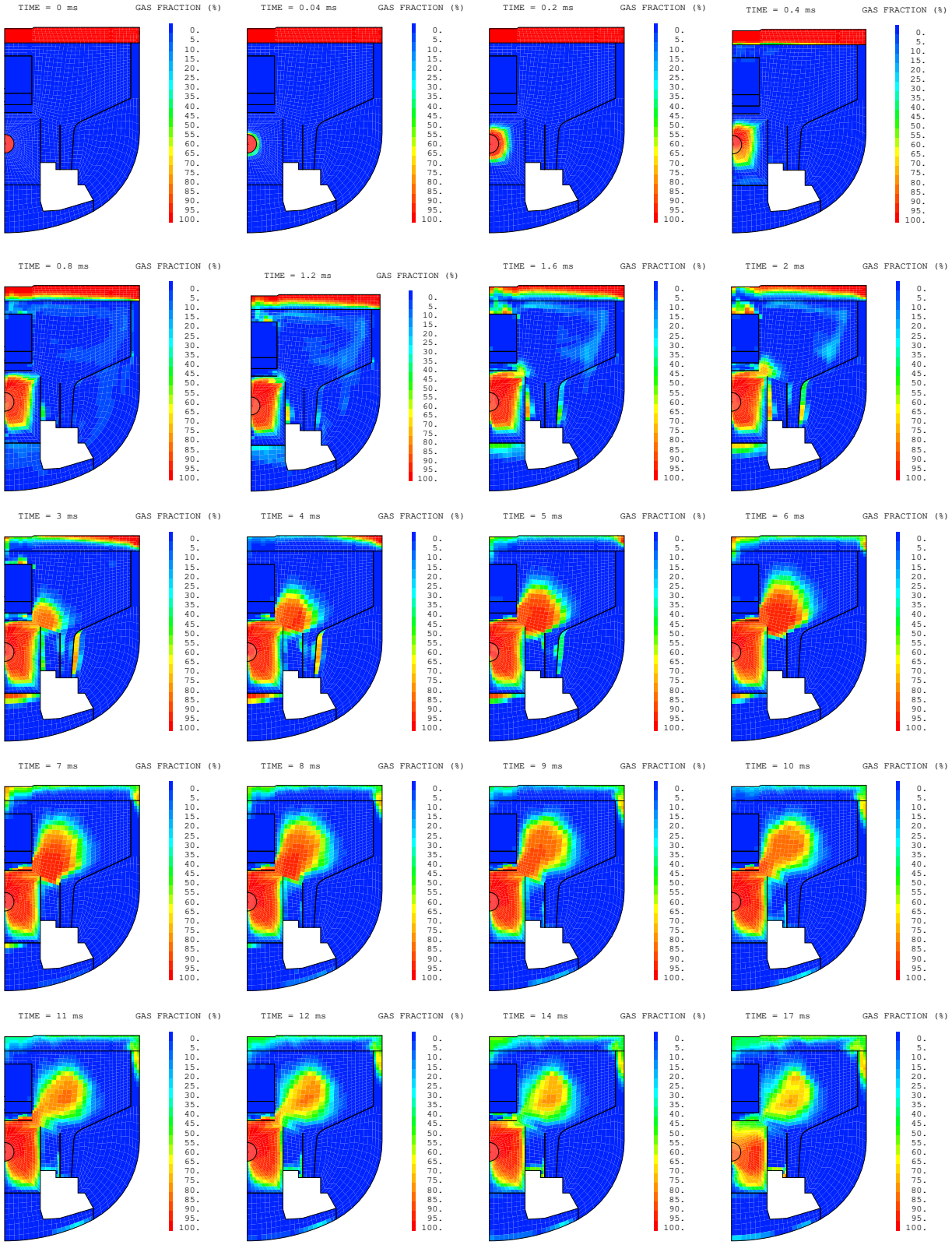

Fig. 3: Gas fraction

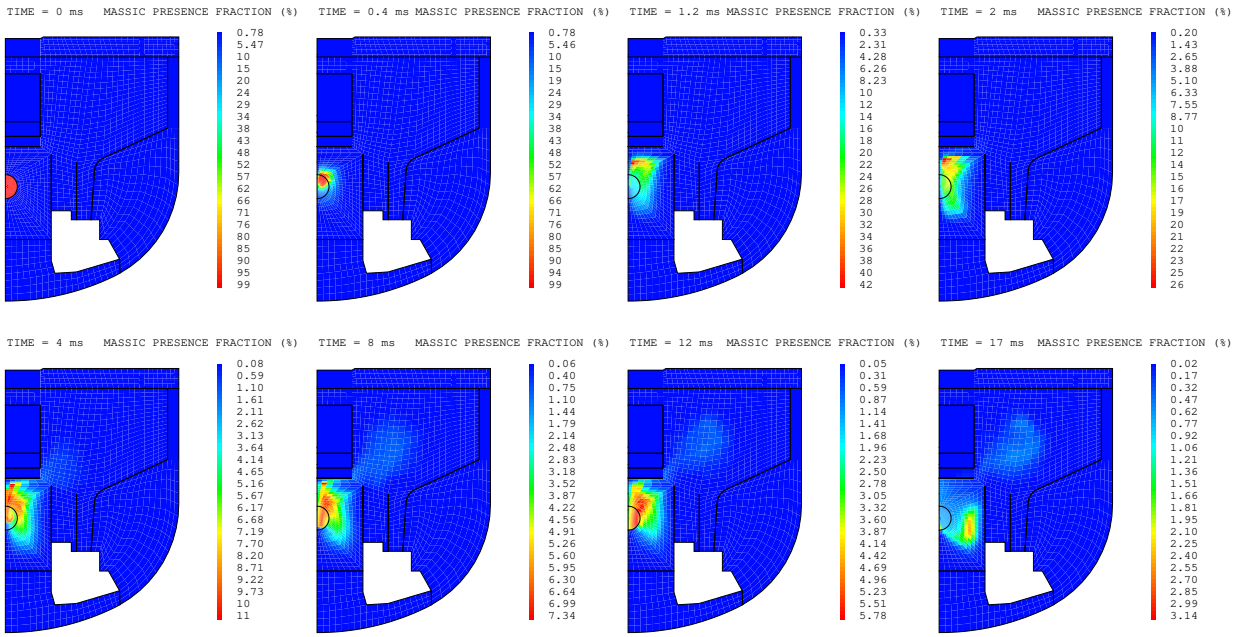

Fig. 4: Bubble massic presence fraction

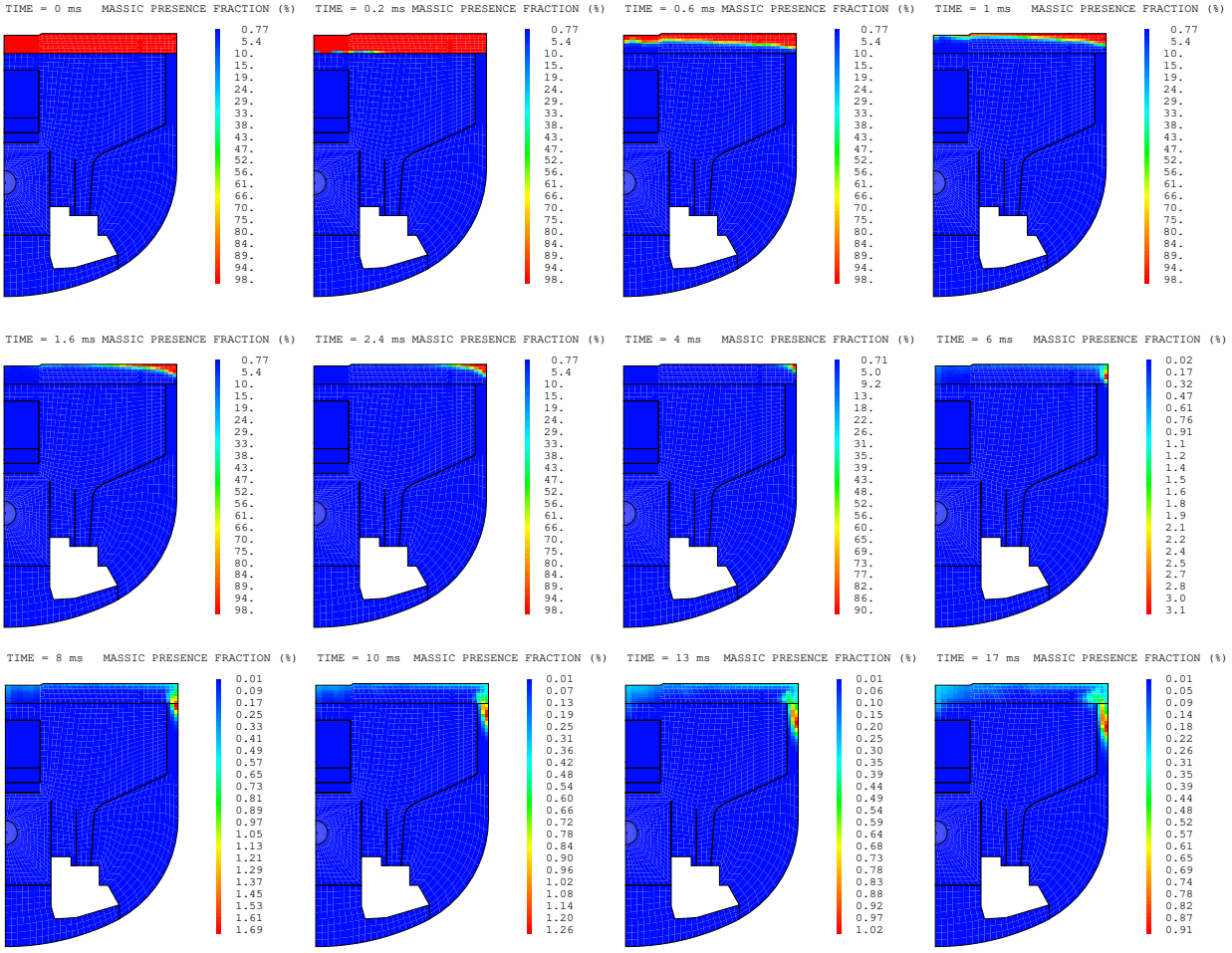

Fig. 5: Argon massic presence fraction

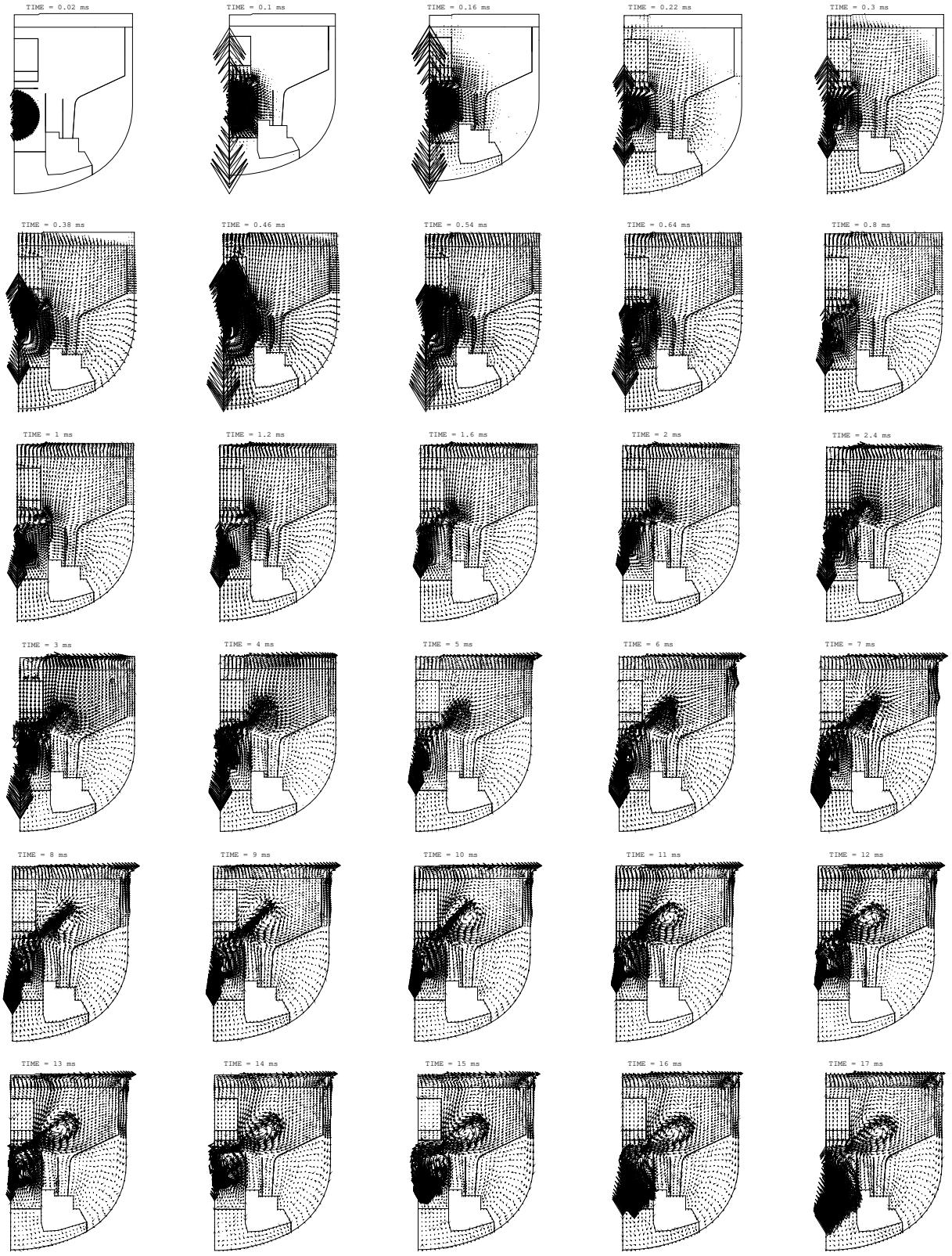

Fig. 6: Fluid speed

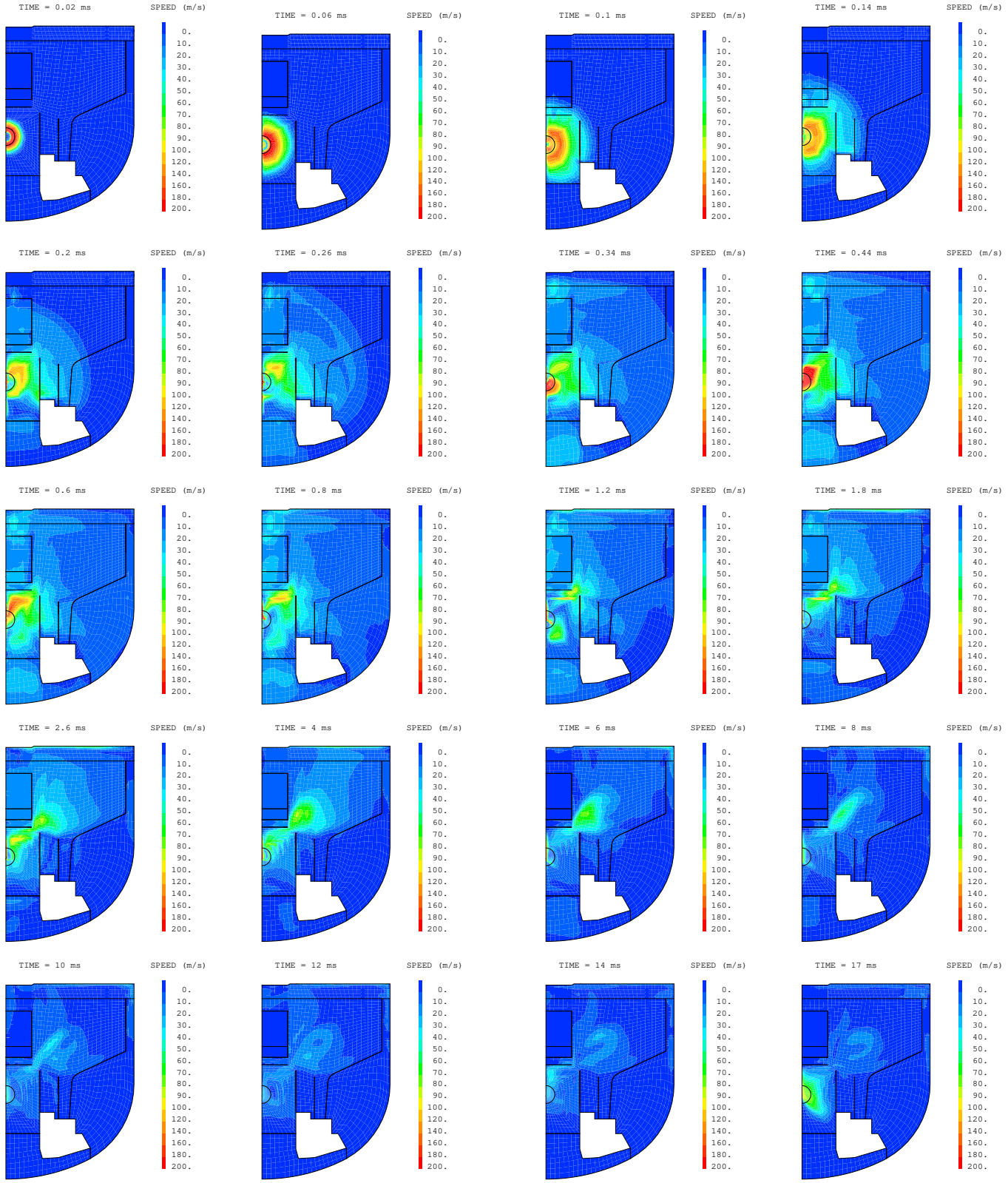

Fig. 7: Fluid speed

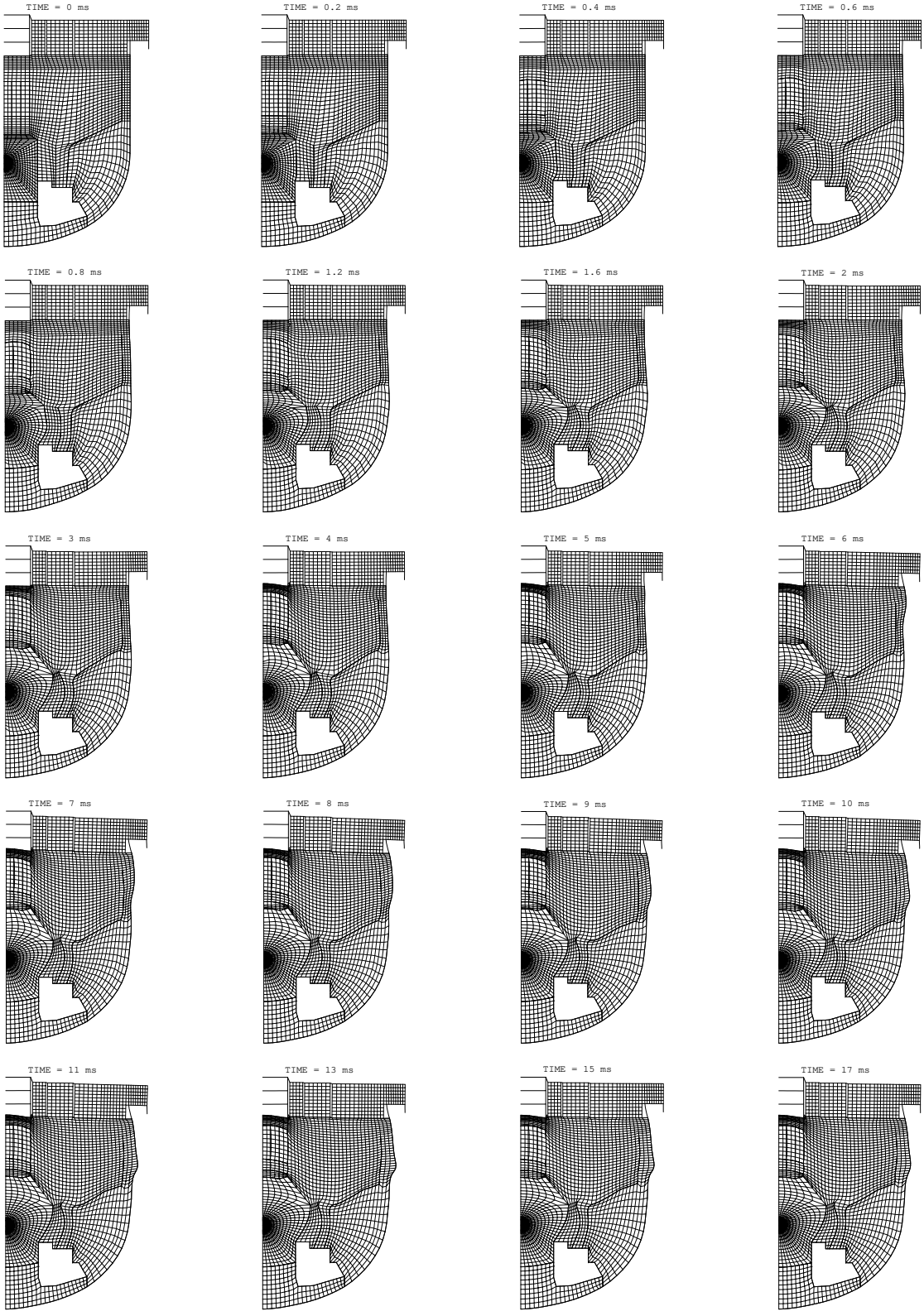

Fig. 8: Deformed shape of the mesh

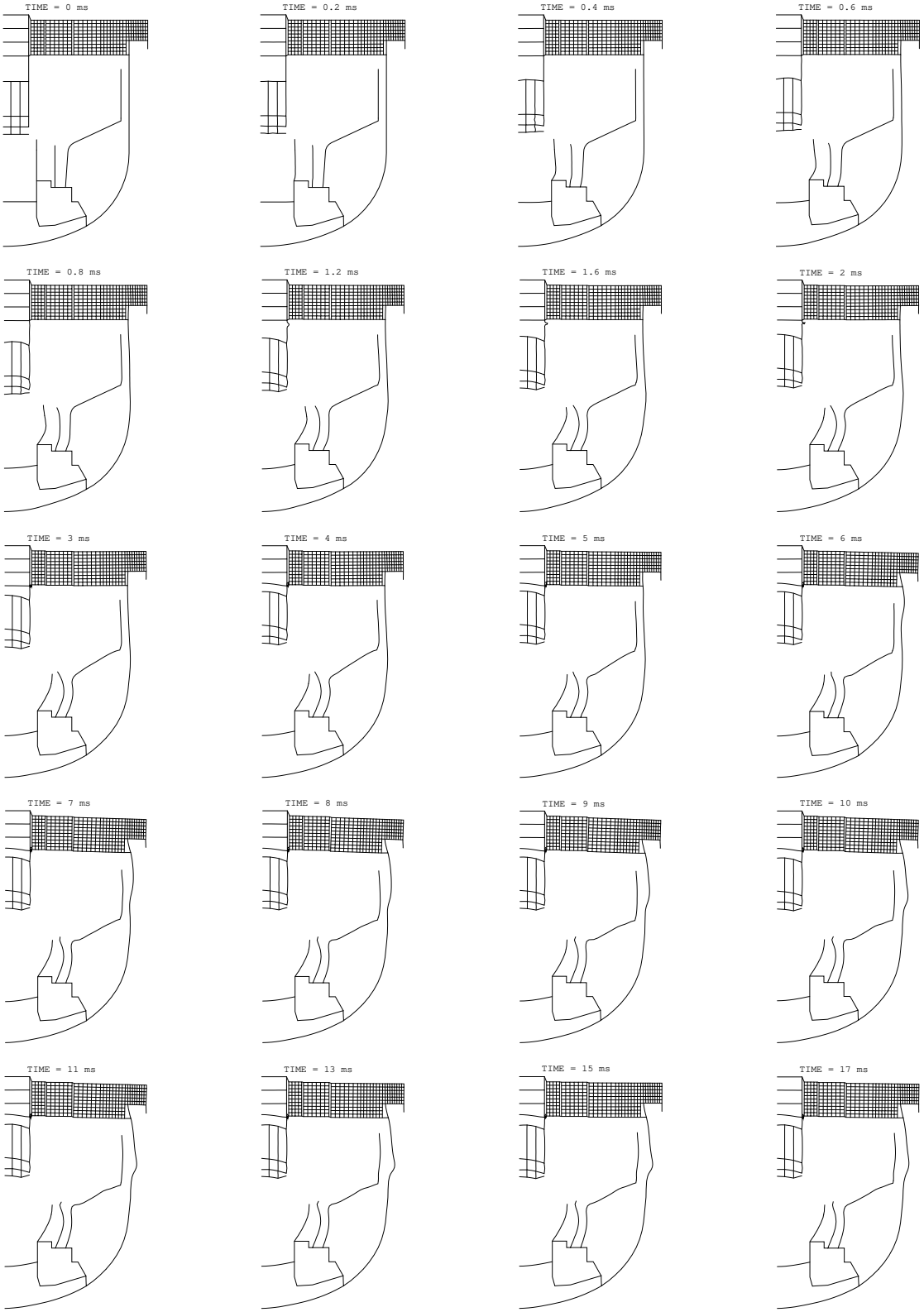

Fig. 9: Deformed shape of the structures

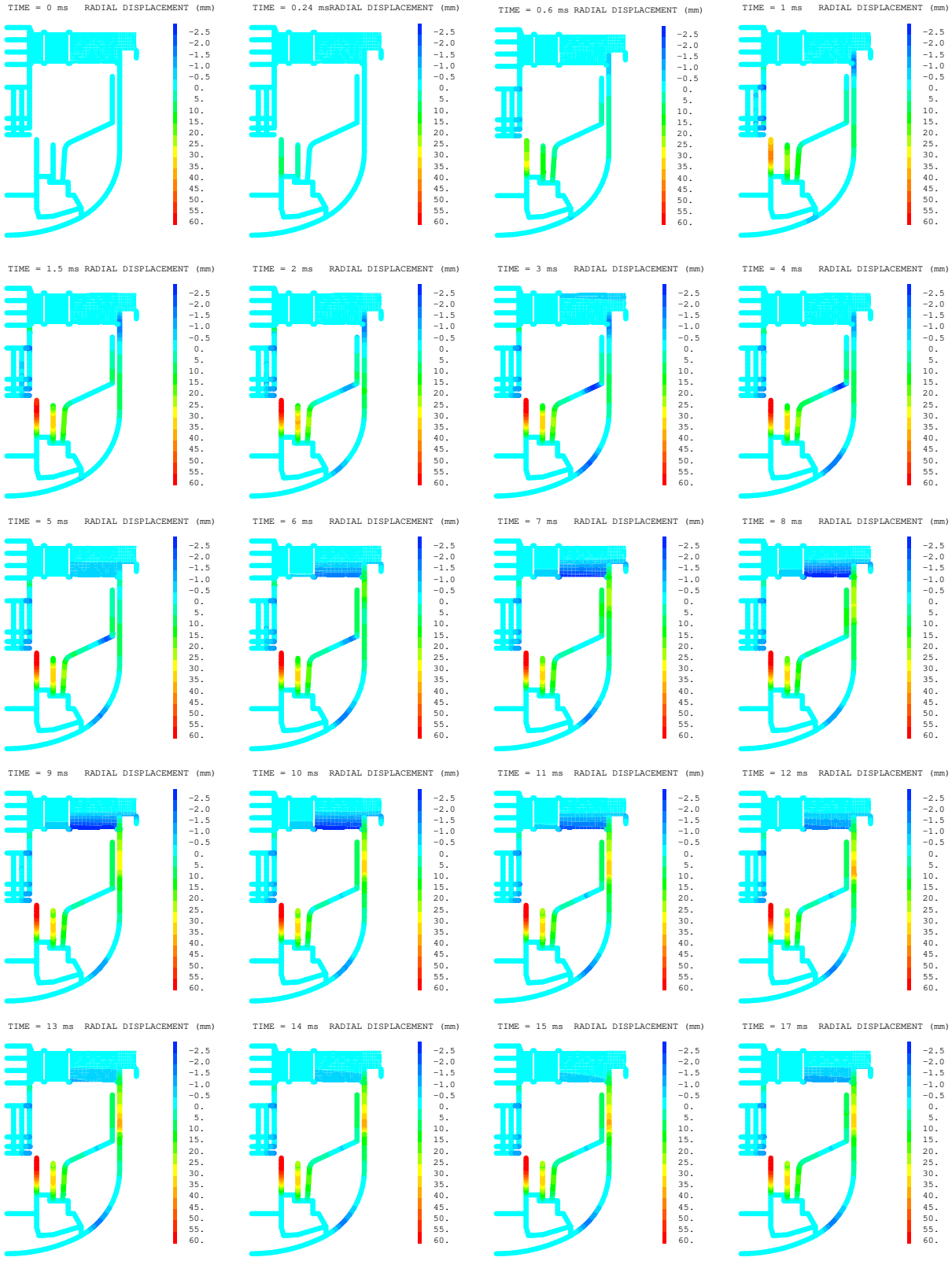

Fig. 10: Radial structure displacements

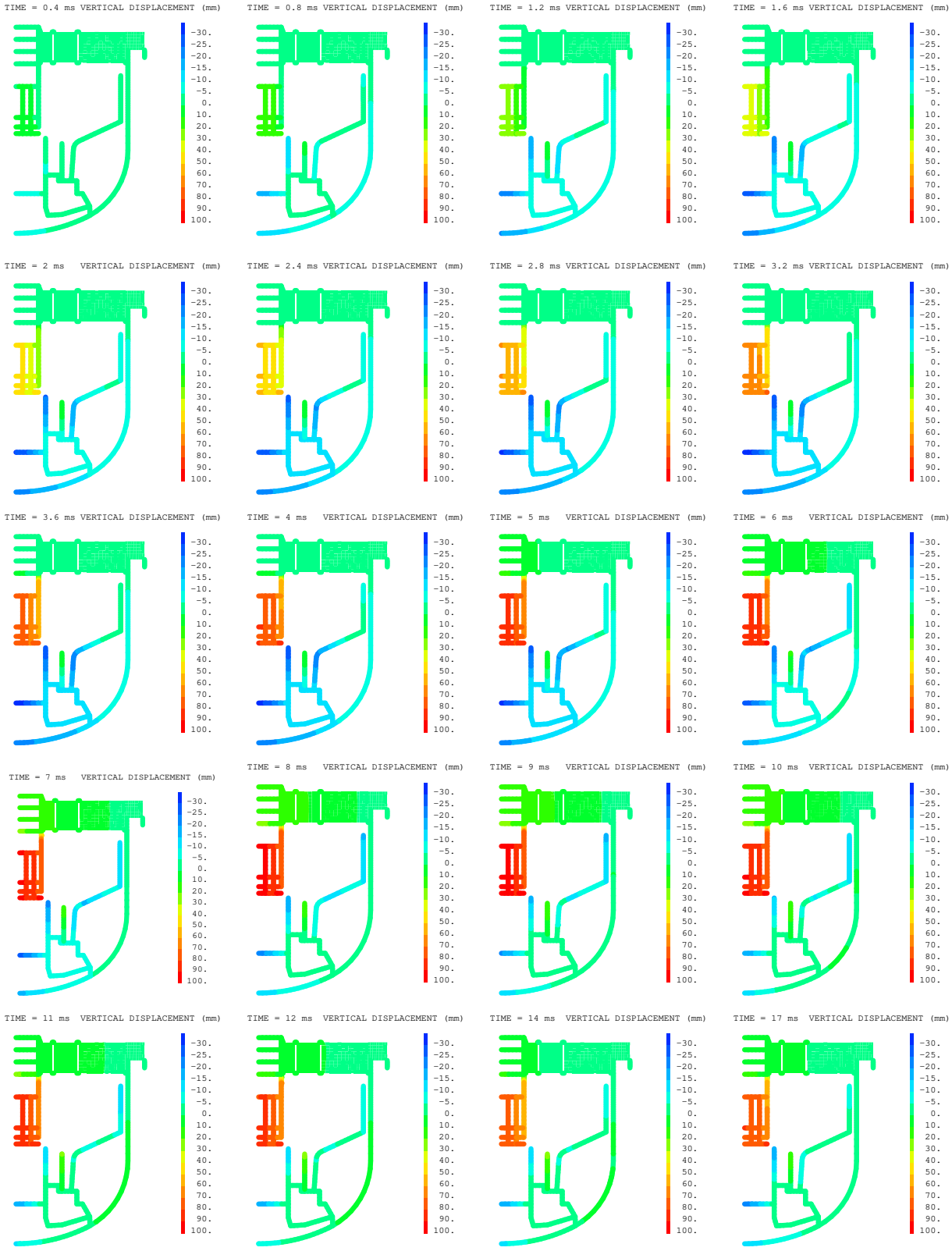

Fig. 11: Vertical structure displacements

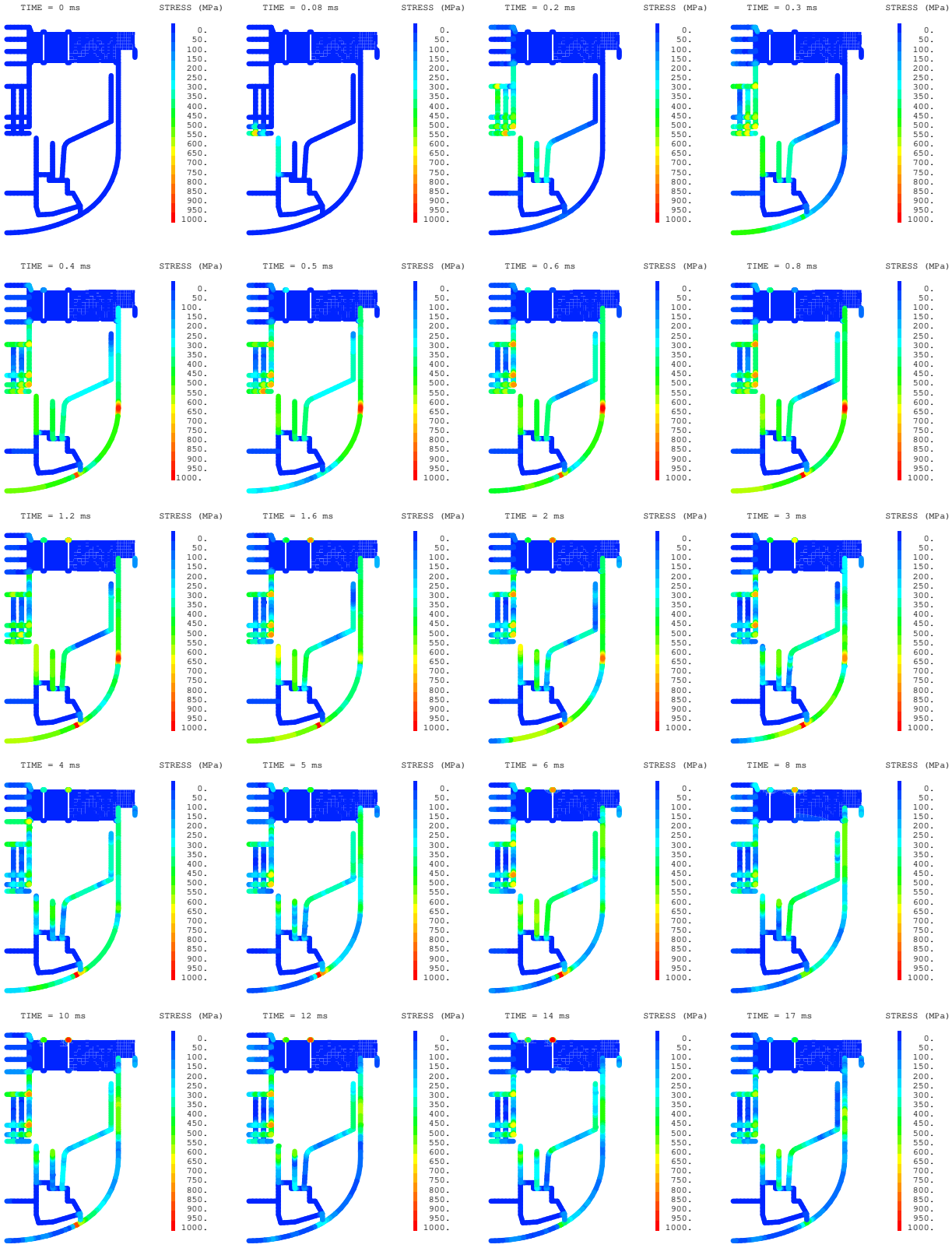

Fig. 12: Von Mises stresses

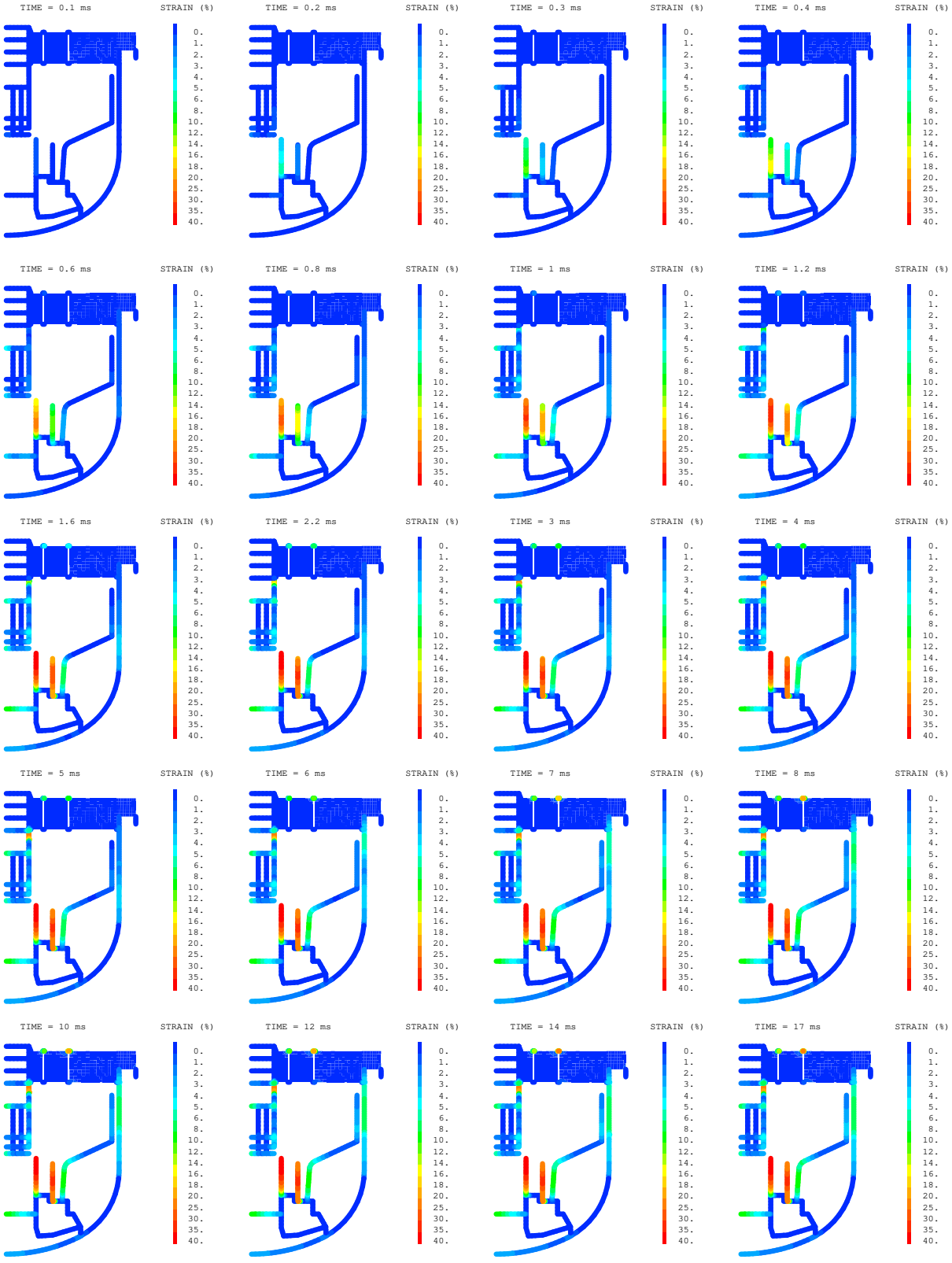

Fig. 13: Plastic strains